



AEOLIAN TRANSPORT OVER A FLAT SEDIMENT SURFACE
by Leo C. van Rijn; www.leovanrijn-sediment.com

- 1. Introduction**
- 2. Modes of wind-blown particle transport and available instrumentation**
- 3. Physics of sand transport by wind**
 - 3.1 Processes**
 - 3.2 Initiation of saltation and critical bed-shear velocity**
 - 3.3 Saltation characteristics**
 - 3.4 Modification of near-surface wind velocity profile**
 - 3.5 Saltation to steady state**
 - 3.6 Total sediment mass flux in saturated conditions**
 - 3.7 Processes affecting sediment transport**
 - 3.8 Dust transport**
- 4. Wind-blown sand transport on beaches**
- 5. Preventive measures to reduce erosion**
- 6. References**



1. Introduction

The wind-driven emission, transport, and deposition processes of sand and dust by wind are termed aeolian processes, after the Greek god Aeolus, the keeper of the winds. Aeolian processes occur wherever there is a supply of granular material and atmospheric winds of sufficient strength: in deserts, on beaches, and in other sparsely vegetated areas, such as dry lake beds. The blowing of sand and dust in these regions helps to shape the surface through the formation of sand dunes and ripples.

The terms dust and sand usually refer to solid particles that are created from the weathering of rocks. Sand is defined as mineral particles with diameters between 63 and 2,000 μm , whereas dust is defined as particles with diameters smaller than 63 μm .

Aeolian sand transport depends on:

- windspeed, direction and duration,
- sand composition (particle size and distribution),
- environmental conditions (moisture, vegetation, beach width, dune height, beach nourishment practices, type of coast: erosive, stabile or accretive).

Many descriptions of the present note are taken from the work of Nickling and Davidson-Arnott (1990), Kok et al. (2012) and Valance et al. (2015).

The file AEOLIANTRANSPORT.xls is used for computations.

2. Modes of wind-blown particle transport and available instrumentation

The transport of particles by wind can occur in several modes, which depend predominantly on particle size and wind speed. As wind speed increases, sand particles of about 100 μm diameter are the first to be moved by fluid drag. After lifting, these particles hop along the surface in a process known as saltation. The impact of these saltators on the soil surface can mobilize particles of a wide range of sizes. Very small particles are predominantly ejected from the soil by the impacts of saltating particles. Following ejection, dust particles are susceptible to turbulent fluctuations and thus usually enter short-term or long-term suspension.

The impacts of saltating particles can also mobilize other particles. However, the acceleration of particles with diameters in excess of about 500 μm is strongly limited by their large inertia, and these particles generally do not saltate. Instead, they usually settle back to the soil after a short hop (< 10 mm) in a mode of transport known as reptation. Alternatively, larger particles can roll or slide along the surface, driven by impacts of saltating particles and wind drag forces in a mode of transport known as creep. Creep and reptation can account for a substantial fraction of the total wind-blown sand flux.

The transport of particles by wind can be crudely separated into several physical regimes (**Figure 2.1**):

- long-term suspension (< 20 μm),
- short-term suspension (20 – 63 μm),
- saltation (63 – 500 μm), and
- reptation and creep (> 500 μm).

Furthermore, we can distinguish between:

- transport-limited saltation, for which the amount of saltating sand is limited by the availability of wind momentum to transport the sand;
- supply-limited saltation, for which the amount of saltating sand is limited by the availability of loose soil particles that can participate in saltation, which can occur for crusted or wet soils.

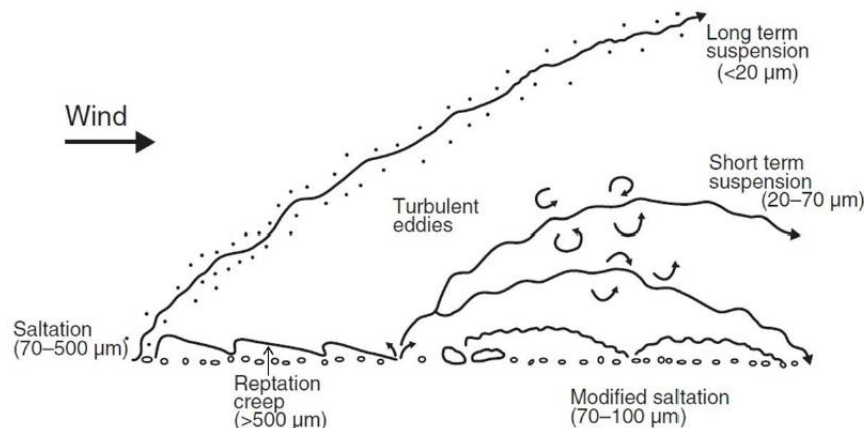


Figure 2.1 Modes of wind-blown transport of sediment (Kok et al., 2012)

Aeolian sand transport can be measured if accurate instrumentation is available. The most basic instruments are:

- wind velocity meter (vane or cup-type sensors);
- electronic grain impact sensors (saltiphones); piezo-electric sensor; laser-type sensor; high-frequency fluctuations can be detected/measured; able to resolve the HF spatial and temporal variability in saltation flux resulting from wind turbulence in the atmospheric boundary layer;
- trap type instruments (Leatherman trap; MCAW trap; BES trap; Streamer trap); one bulk sample over the test duration is obtained.

A saltiphone is a commercially available sampler which consists of a microphone installed in a stainless-steel tube mounted on a ball bearing (Figure 2.2C; Poortinga et al., 2013). Sand particles that hit the microphone produce a high-frequency signal. Frequencies of about 8 KHz are amplified and used to determine saltation whereas other frequencies that are caused by rain and wind are reduced using a narrow band filter. Two output signals are provided: a digital pulse and an analogue voltage. The digital signal gives an output that is translated into number of counts. The analogue output signal also provides this information but has the additional option of measuring the intensity of particle impacts because it measures the energy of impact on the membrane. In this mode, the output signal represents the kinetic energy of the particles, and thus particle size and speed. Calibration is required to relate the output variables to sand transport rates. Calibration problems are the accuracy of input reference conditions (other trap-type sampler co-located beside the sensor), the saturation effects, the sensitivity of each microphone affecting the acoustic signal and the cleanliness of the output signal (noise ratio).

A similar type of sensor is the piezo-electric sensor which generates an electric pulse when a saltating particle hits the piezoelectric element.

Laser-based systems use a laser beam and photo sensors to detect sediment particles crossing the laser beam.

Various trap-type samplers are available (Poortinga et al., 2013). The original Wilson and Cooke trap consists of a bottle containing an inlet and outlet, whereby the trapped sediment is deposited in the bottle. In later studies, these bottles were mounted on a pole equipped with a sail to ensure that the inlet was always directed towards the wind (Figure 2.2A). This extended setup is called the Modified Wilson and Cooke (MWAC) trap. The MWAC-traps showed good performance in a wind tunnel study (Poortinga et al. 2103). The MWAC- trap may be problematic to use at coastal beaches in strong winds with rain and salt sprays leading to blocking/clogging of the small intake openings (De Grande and De Moor, 2019). Bottles/traps close to beach surface may easily generate small scour holes and can therefore not be used close to the sand surface, where most of the sand is moving.



The trap of Basaran and Erpul (BEST) is a cyclone-type trap with a conical shape (**Figure 2.2B**). Sediment enters the trap via an inlet and follows a circular trajectory within the cone. The heaviest particles will settle due to gravitational and centrifugal forces whereas the lightest particles will be evacuated through the outlet. The Sherman streamer trap (SST) is a simple trap with a nylon bag (50 or 63 μm) wherein the sand particles are trapped, see **Figure 2.2D**. This trap system (Sherman et al., 2014) is comprised of a vertical stack of thin stainless-steel rectangular frames enclosed with nylon mesh that maximizes flow through the trap while minimizes flow distortion. The nylon mesh can be adhered to the thin metal frame via spray adhesive. This cost-effective set of traps is easy to use, quick to deploy, easy to retrieve samples in the field and have excellent efficiency (Sherman et al., 2014), (Farrell and Swan, 2016).

The efficiency and behavior of different sediment traps were reported in numerous studies. Most of these studies used the controlled environment of a wind-tunnel, but some also performed a relative calibration in the field (Poortinga et al., 2013).

Basaran et al. (2016) compared two trap-type samplers at a field site in Turkey: BEST and MWAC. They found that the BEST was able to trap both sand and dust size particles up to 1.20 m above soil surface. The MWAC was not able to adequately trap sand particles.

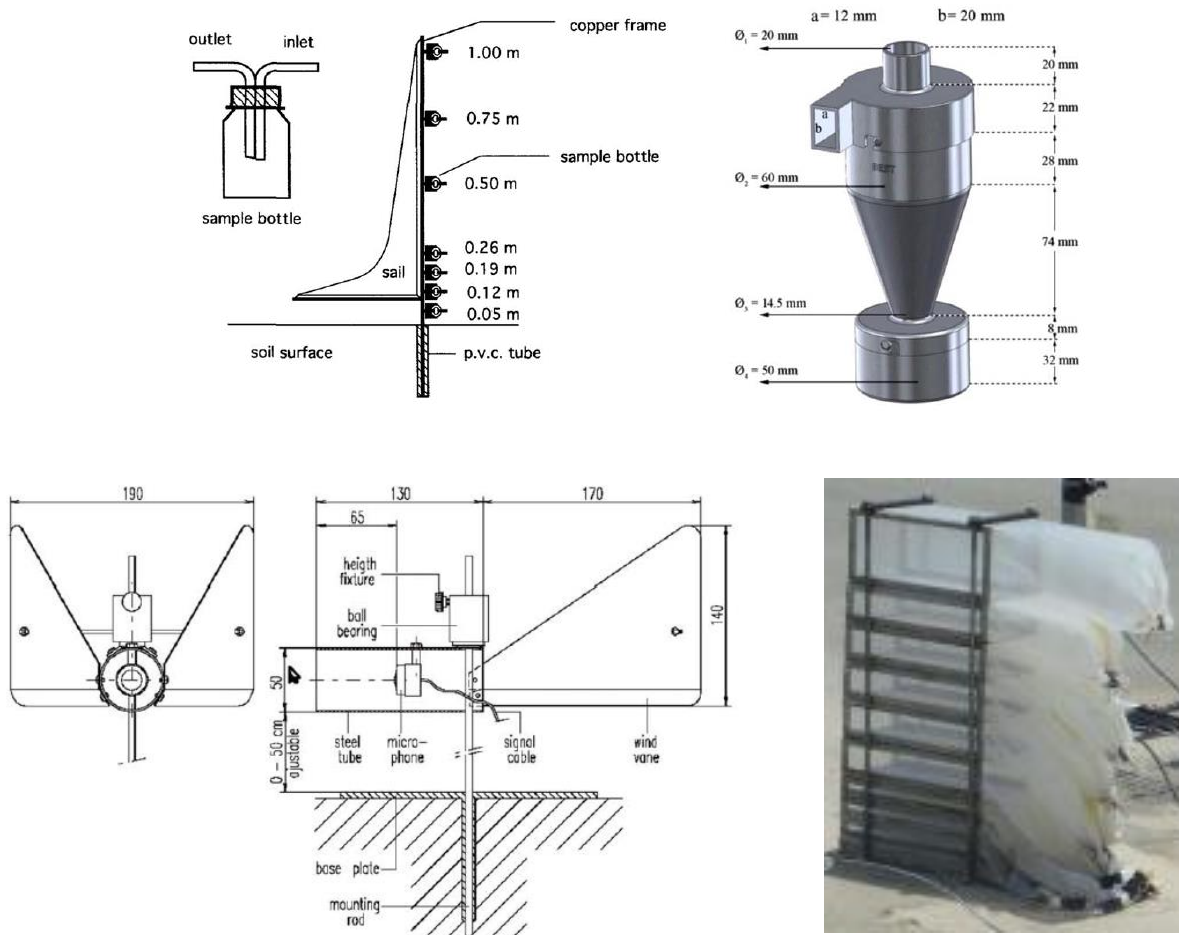


Figure 2.2 Instrumentation for aeolian sand transport (Poortinga et al., 2013)
Upper left: Modified Wilson-Cook trap (MWAC); Upper right: Basaran-Erpul Sediment trap (BEST)
Lower left: Salthophone sensor; Lower right: Sherman Streamer trap (SST)



3. Physics of sand transport by wind

3.1 Processes

3.1.1 Saltation of particles

Saltation plays a central role in aeolian processes. Saltation is initiated when the wind stress is sufficient to lift surface particles into the wind stream, which for loose sand occurs around a wind speed of 4 to 6 m/s. Following initiation, the lifted particles are accelerated by wind into ballistic trajectories and the resulting impacts on the soil bed can eject, or splash, new saltating particles into the wind stream. This process produces an exponential increase in the particle concentration, which leads to increasing drag on the wind, thereby retarding the wind speed in the saltation layer. It is this slowing of the wind that acts as a negative feedback by reducing particle speeds, and thus the splashing of new particles into saltation, which ultimately limits the number of saltating particles and thereby partially determines the characteristics of steady state saltation.

The physics of aeolian saltation can be roughly divided into four main physical processes:

- the initiation of saltation by the aerodynamic lifting of surface particles (threshold/critical shear velocity),
- the subsequent trajectories of saltating particles,
- the splashing of surface particles into saltation by impacting saltators, and
- the modification of the wind profile by the drag of saltating particles.

3.1.2 Moisture content and cohesion

Wind-induced sand transport is strongly affected by moisture content and related cohesion.

Cohesion between particles increases the surface resistance against erosion (critical shear velocity). Cohesion may result from the presence of moisture, salt, algae, clay, organic matter and carbonate. Moisture content may be the direct result of precipitation or capillary action (adhesive forces; surface tension forces).

Moisture fraction is generally defined as: $mc = \text{mass water of sample} / \text{mass dry sand of sample}$.

Moisture content is moisture fraction $\times 100\%$

Moisture content of a saturated sample can be computed by the expression $mc_{\text{saturated}} = [\varepsilon / (1 - \varepsilon)] [\rho / \rho_s] \times 100\%$ with: $\varepsilon =$ porosity factor (0.35-0.45 for sand); $\rho =$ water density ($\cong 1000 \text{ kg/m}^3$); $\rho_s =$ sand density ($\cong 2650 \text{ kg/m}^3$). yielding $mc_{\text{saturated}} = 20\% - 30\%$. Generally, moisture contents are in the range of 0 to 10%, as the pores are not fully saturated with water.

Let us assume that a sand particle with diameter D is covered by a thin water film with thickness δ except at the particle contact points; any other pore water is absent.

The volume of the water film is: $V_{\text{wfi}} = 1.33\pi [(0.5D + \delta)^3 - (0.5D)^3]$ and the mass is: $M_{\text{wfi}} = \rho V_{\text{wfi}}$.

The volume of the sand particle is: $V_{\text{sand}} = 1.33\pi (0.5D)^3$ and the mass is $M_{\text{sand}} = \rho_s V_{\text{sand}}$.

The mass ratio of water and dry sand defined as the moisture fraction is:

$$mc = M_{\text{wfi}} / M_{\text{sand}} = \rho [(0.5D + \delta)^3 - (0.5D)^3] / [\rho_s (0.5D)^3].$$

Using: $D = 200 \mu\text{m}$ for sand, $\delta = 0.01D = 2 \mu\text{m}$, it follows that: $mc \cong 0.025$ (2.5%).

Thus, a thin water film with thickness equal to $2 \mu\text{m}$ surrounding a sand particle of $200 \mu\text{m}$ yields a moisture content of about 2.5%. A water film of $1 \mu\text{m}$ yields a moisture content of 1%. Dry sand has a moisture content $< 0.25\%$ (Han et al., 2011).

In situations with a moisture content $> 2.5\%$, the sand transport rate is strongly reduced to a very small value (see **Figure 3.12**). In situations with $mc = 10\%$ (near the water line), the surface is so saturated that aeolian transport reduces to almost zero even under very strong winds.



Small amounts of moisture are characteristic of beach sediments with moisture being created from a variety of sources, including wave uprush, capillary rise from the subsoil water table, wave spray and precipitation (rain fall). Field experiments (Davidson-Arnott, 2007) show that the moisture content at a certain location and thus the critical shear velocity can change over a period of minutes to hours through drainage as the beach water table falls or drying by wind and solar radiation. Surface moisture can limit the rate of release of sediment from the surface, even when sediment transport is continuous, and that it is probably the primary control on the observed adjustment effects on beaches. Even low levels of moisture may effectively reduce the maximum transport rate, i.e. the final transport rate may never reach levels predicted for dry sand.

Based on this, the wind-driven sediment transport is highly variable in space and usually intermittent in time. Moisture increases the resistance of the sand particles against lift and drag, due to cohesive forces of the adsorbed water films surrounding them.

The effects of rainfall on sediment transport by wind are twofold:

1. intensive wind-driven rain can transport sediment by combined splash and saltation processes;
2. residual moisture increases the cohesive forces between particles and therewith the resistance of the sediment against lift and drag.

On sandy beaches, the first process is significant over short time intervals during high-intensity rain events, but this effect is, in terms of quantity, of secondary importance. The second process effect of residual moisture resulting from rainfall lasts over longer time spans and is of crucial importance yielding a significant reduction of critical shear velocity and hence sediment transport.

The field work of Davidson-Arnott et al. (2007) at a Canadian beach with sand of 0.26 mm shows large variations of the critical wind speeds: $U_{wind,cr,min} = 5$ m/s (lowest wind speed with sediment transport) and $U_{wind,cr,max} = 9$ m/s (highest wind speed without sediment transport) mainly due to variations of the moisture content.

The mean critical wind speed is equal to about $\cong 0.5(U_{wind,cr,min} + U_{wind,cr,max})$ and is found to increase with moisture content (about 30% for a moisture content increasing from 0 to 4%).

Davidson-Arnott et al. (2007) have proposed to consider a distribution of threshold values (rather than a single value) with $U_{cr,min}$ and $U_{cr,max}$ as the extremes for dry and moist sand (**Figure 3.1**). When the beach is dry, the distribution would probably reflect in some way the particle size distribution. When the beach surface is quite moist the whole distribution will shift towards much higher threshold wind speeds and the shape of the distribution may change to include the influence of cohesion processes. The shape of the distribution for the moist surface should also reflect the potential for surface drying. Incident winds also fluctuate in strength and thus have their own probability distribution, as shown in Figure 3.5. The resulting temporal pattern of sediment entrainment thus reflects the relationship between the two probability curves: one for wind speed and the other for the entrainment threshold. In **Figure 3.1** the threshold distribution for relatively dry sand lies mostly below that of the wind-speed distribution resulting in only a small fraction of time when the speed dropped below the threshold (nearly continuous sediment transport). However, with a relatively moist surface, entrainment will take place only when there is coincidence between higher wind gusts and surface drying shown by the small area of overlap between the two curves on the right-hand side of **Figure 3.1** (only occasional sediment transport).

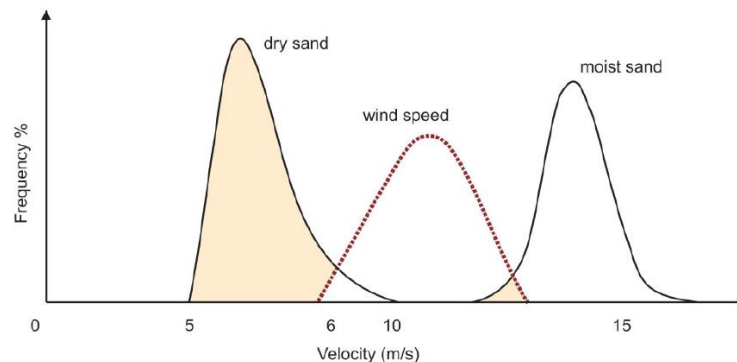


Figure 3.1 Sketch of probability distribution of the critical wind speed for dry and moist sand (Davidson-Arnott et al. 2007)

3.1.3 Vegetation

Vegetation leads to an increase of the aerodynamic roughness length (z_o), and to an increase of the friction velocity above the vegetation layer. In the vegetation layer itself, momentum is extracted from the air flow and turbulence is produced at the lee side of the roughness elements. The surface friction velocity (u_*) depends on the vegetation physiography, and on the density and spatial configuration of the plants/stems, which can be described by a reduction factor (Equation 3.9; $\alpha_{veg}=1$ for a flat surface without vegetation; $\alpha_{veg}=0.5$ for plants of 0.1 m high and 5 per m^2 ; $\alpha_{veg}=0.2$ for plants of 0.2 m high and 15 per m^2).

3.1.4 Shells

Shells (calcium carbonate) can protect the beach surface against erosion of the sand particles. Van der Wal (1999) studied the effect of shells on the wind-induced transport rate of beach sand. Beach sand samples were taken from 5 sites along the Dutch coast and tested in a wind tunnel. The d_{50} varied in the range of 0.21 to 0.35 mm. The percentage of shells (> 2 mm) varied in the range 1 to 30%. A tray with (length=1.22m; width=0.33 m; height=0.03m) was filled with weighed oven-dried sand and placed in the middle of the test section. The sample surface was smoothed and levelled to the tray edges. The wind speed was gradually increased over one minute to about 11 m/s and kept at this speed for another minute. Then, the wind speed was gradually returned to zero over one minute. After the experiment, the sand was reweighed. The percentage of sand blown off during the test was calculated for each of the experiments. The transport rate was reduced by a factor of 1.5 for samples with a percentage of shells of 10% and by a factor of 3 for samples with a percentage of shells of 20% to 30%. Shell pavements were formed during the wind tunnel experiments with shell-rich beach samples. Samples containing very coarse gravels and stones also showed pavement effects. This effect can be crudely represented by a reduction factor $r=(1-2p_{shell}/100)^2$ with p_{shell} =percentage of shell. Large percentages of shell are mostly found on the upper part of natural beaches outside the wave action zone and on beaches with nourished sand.

Cadée (1992) has done observations of aeolian transport of large shells (Mya shells) along the Prins Hendrik sea dike on the island of Texel (The Netherlands) during and after storm events with wind velocities $>$ Beaufort 10.

His observations are summarized, as follows:

- storm event from South with wind velocities > 30 m/s (BF 12) on 25 January 1990: large quantities of Mya-shells (lengths of 30 to 110 mm; mean length of 60 mm) were transported from the narrow beach on the seaside across the dike and were deposited on the landward side of the dike.
- storm event from Southwest with wind velocities > 30 m/s (BF 12) on 26 February 1990: Mya-shells and other shells were transported over the narrow beach parallel to the dike through saltations with maximum height of 1 m and maximum length of 10 m; shells lying with their hollow side to the beach



surface (convex upward) were very stabile and hardly movable; shells with their rounded side to the beach (convex downward) were very mobile.

- storm event from South in January 1991 with wind velocities of 24 to 27 m/s (BF 10): Mya-schells were transported across the dike.

Based on this, it can be concluded that large shells can only be transported in appreciable quantities during storm events with relatively high wind speeds (BF > 10). The critical wind speed at the onset of motion of large Mya-shells is about 20 m/s ($u_{*,cr}=0.75$ m/s).

3.2 Initiation of saltation and critical bed shear velocity

Saltation is initiated by the lifting of a small number of particles by wind stress. The value of the wind stress at which this occurs is termed the fluid or static threshold. This threshold depends not only on the properties of the fluid, but also on the gravitational and interparticle cohesion forces that oppose the fluid lifting. The fluid threshold is distinct from the dynamic or impact threshold, which is the lowest wind stress at which saltation can be sustained after it has been initiated. The impact threshold is smaller than the fluid threshold because the transfer of momentum to the surface through particle impacts is more efficient than through drag.

An expression for the fluid threshold can be derived from the force balance of a stationary surface particle (Bagnold 1941), yielding:

$$u_{*,cr} = \alpha_{cr} \alpha_{mois} [(\rho_s / \rho_{air} - 1)g d]^{0.5} \quad \text{for } d_{50} > 100 \mu\text{m} \quad (3.1a)$$

$$u_{*,cr} = \alpha_{mois} u_{*,cr,100\mu\text{m}} \quad 20 < \text{for } d_{50} < 100 \mu\text{m} \quad (3.1b)$$

$$U_{wind,cr} = (u_{*,cr} / \kappa) / \ln(30h_{wind} / k_s) \quad (3.2)$$

with:

ρ_{air}	= density of air ($\cong 1.2$ kg/m ³);
ρ_s	= sediment density (2650 kg/m ³);
g	= acceleration of gravity (m/s ²);
u^*	= surface shear velocity due to wind forces (m/s);
$u_{*,cr}$	= surface shear velocity at initiation of motion, threshold shear velocity (m/s);
k_s	= equivalent roughness length scale of Nikuradse (m);
U_{wind10}	= wind velocity at 10 m above the surface (m/s);
h_{wind}	= height at which wind velocity is defined (= 10 m);
κ	= constant of Von Karman (=0.4);
α_{cr}	= 0.11 based on data of Shao-Lu (2000) and Han et al. (2011); $\cong 0.1$ based on Bagnold (1941);
α_{mois}	= moisture coefficient (> 1);

Figure 3.2 shows the measured and computed data of Bagnold and others. Measurements of the fluid threshold for sand and dust are denoted by filled symbols, whereas measurements of the fluid threshold for materials other than sand and dust are denoted by open symbols.

Figure 3.3 shows the Bagnold-expression for particles in the range of 0.1 to 1 mm.

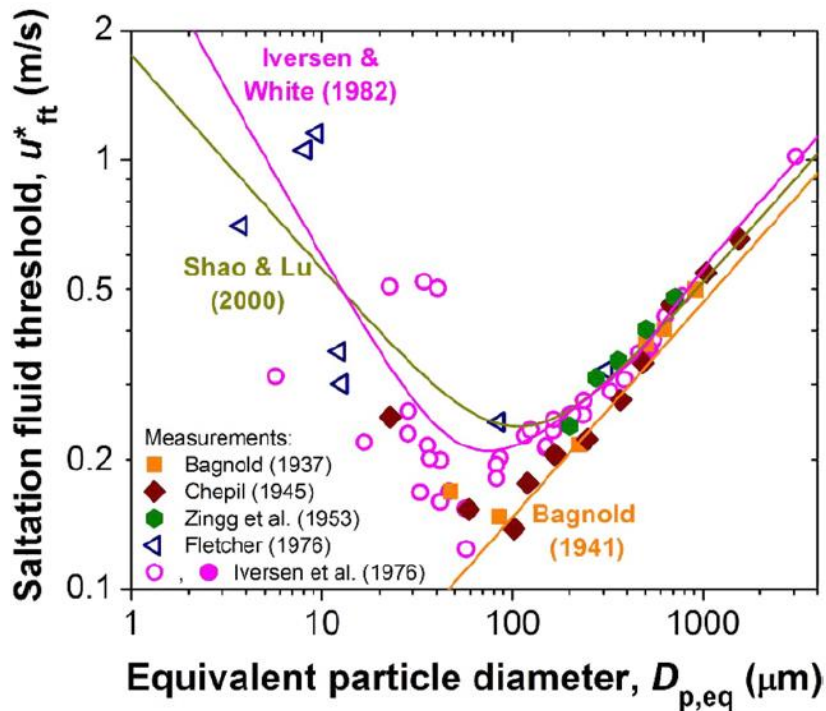


Figure 3.2 Threshold shear velocity (Kok et al., 2012)

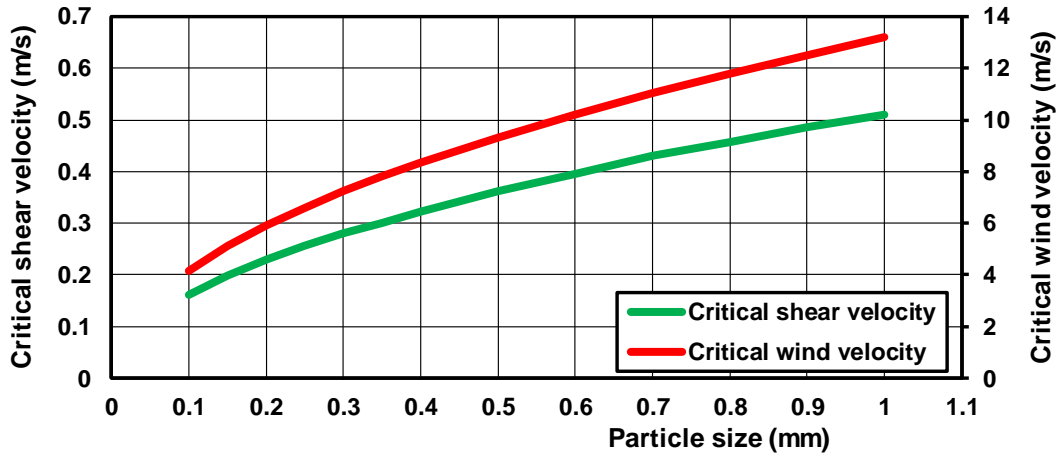


Figure 3.3 Critical shear velocity and critical wind velocity of dry, loose sand particles ($k_s = 0.01$ m, $h_{wind} = 10$ m, $\kappa = 0.4$, $\alpha_{mois} = 1$, $\rho_{air} = 1.2$ kg/m³)

Han et al. (2011) studied the effect of moisture content on the critical shear velocity, see Figure 3.4. The effect of moisture is negligibly small for moisture content < 0.25%. Table 3.1 shows critical shear velocity values for dry sand and low values of the moisture content (0.25% and 0.5%). The results of Han et al. (2011) for almost dry sand with $mc = 0.25\%$ are slightly larger (factor 1.1 to 1.3) than that of Bagnold (1941). Sand with $mc = 0.5\%$ has a significant higher critical shear velocity (factor 1.5 to 2). For $mc = 2.5\%$ the critical shear velocity is factor of 3 higher than that for $mc = 0.25\%$, see Figure 3.3.

The effect of the moisture content on the critical shear velocity can roughly be represented by $u_{*wet} = \alpha_{mois} u_{*dry}$ with: $\alpha_{mois} = 1 + 2 \tanh(mc - 0.25)$ and $mc =$ moisture content in % and $\alpha_{mois} = 1$ for $mc \leq 0.25\%$ (dry sand), see Figure 3.4.



Particle size (μm)	Critical shear velocity based on Bagnold (1941) dry sand (m/s)	Critical shear velocity (m/s) based on Han et al. (2011)	
		mc=0.25% (almost dry sand)	mc=0.5%
110	0.17	0.23	0.38
140	0.19	0.25	0.40
175	0.21	0.27	0.42
250	0.26	0.30	0.52
350	0.30	0.35	0.65
450	0.34	0.35	0.67

Table 3.1 Comparison of critical shear velocities of Bagnold (1941) and Han et al. (2011) for dry sand and sand with low moisture contents

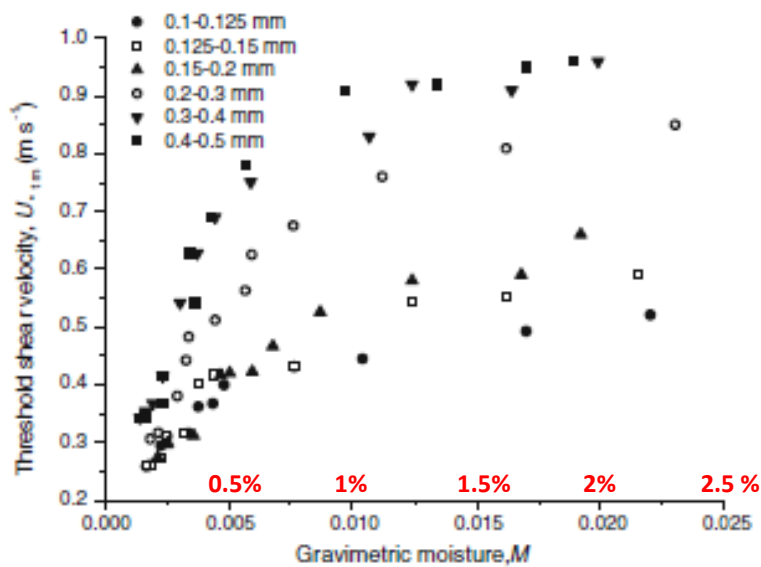


Figure 3.4 Threshold shear velocity as function of grain diameter and moisture content (Han et al., 2011)

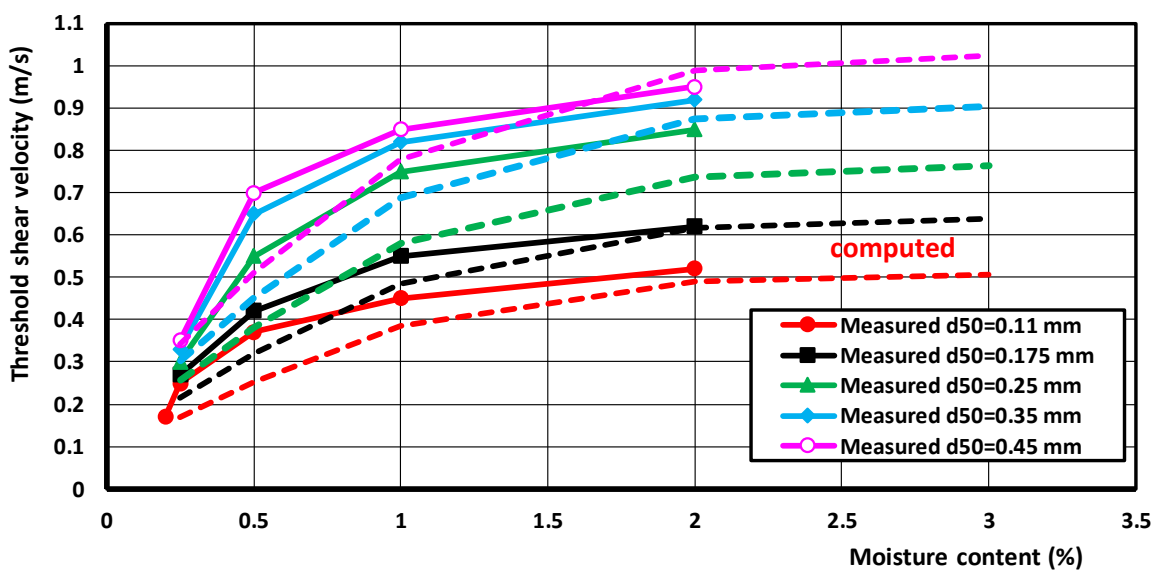


Figure 3.5 Threshold shear velocity as function of particle diameter and moisture content; measured data of Han et al. (2011) and computed values based on Eq. (3.1) with $\alpha_{cr}=0.11$



3.3 Saltation characteristics

After saltation has been initiated, lifted sand particles undergo ballistic trajectories that are determined primarily by the gravitational and aerodynamic drag forces. The acceleration of particles by the drag force transfers momentum from the fluid to the saltating particles and thus retards the wind profile in the saltation layer.

Numerical computer simulations show saltation heights of 15 to 30 mm and saltation lengths of 200 to 500 mm for particles in the range of 100 to 500 μm under a wind speed of about 10 m/s ($u_* \approx 0.4$ m/s). Saltation heights are about 50 mm for a wind speed of 25 m/s.

The ballistic trajectories of saltating particles are terminated by a collision with the surface. These particle impacts onto the soil surface are a critical process in saltation for two reasons. First, the splashing of surface particles by impacting particles is the main source of new saltators after saltation has been initiated. And second, since particles strike the soil nearly horizontally and rebound at angles of about 40° from horizontal, the impact on the soil surface partially converts the saltator's horizontal momentum gained through wind drag into vertical momentum. This conversion is critical to replenish the vertical momentum dissipated through fluid drag.

The impact of a saltating particle on the soil bed can thus produce a rebounding particle as well as one or more splashed particles.

3.4 Modification of near-surface wind velocity profile

The wind velocity without particles can be described by: $U_{\text{wind},z} = (u_*/\kappa) \ln(z/z_0)$ (3.3)

where $\kappa = 0.40$ is von Kármán's constant, z_0 is the aerodynamic surface roughness, which denotes the height at which the logarithmic profile, when extrapolated to the surface, yields zero wind speed.

The large length scale of the atmospheric boundary layer in which saltation occurs causes the Reynolds number of the flow to be correspondingly large, typically in excess of 10^6 such that the flow in the boundary layer is turbulent. Since the horizontal fluid momentum higher up in the boundary layer exceeds that near the surface, eddies in the turbulent flow on average transport horizontal momentum downward through the fluid. Together with the much smaller contribution due to the viscous shearing of neighboring fluid layers, the resulting downward flux of horizontal momentum constitutes the fluid shear stress. Because the horizontal fluid momentum is transported downward through the fluid until it is dissipated at the surface, the shear stress is approximately constant with height above the surface for flat and homogeneous surfaces.

Equation (3.3) is based on the assumption that the shear stress in the surface layer is constant with height. This is a realistic approximation for flat, homogeneous surfaces, but can be unrealistic for other conditions, such as for surface with non-uniform surface roughness or substantial elevation changes. Furthermore, the drag by saltating particles reduces the horizontal momentum flux carried by the wind.

For small roughness-related Reynolds numbers (< 5), the roughness elements are too small to substantially perturb the viscous sublayer of about 0.4 mm, and the flow is termed aerodynamically smooth.

For large roughness-related Reynolds numbers (> 60), the roughness elements are so high that the viscous sublayer is substantially disrupted, and the flow is termed aerodynamically rough and $z_0 = k_s/30$.

Aeolian saltation on Earth takes place for roughness-related Reynolds numbers of 1 to 100 and thus usually occurs in the transition zone between the smooth and rough aerodynamic regimes. Since the roughness in



the transition regime does not differ much from that in the aerodynamically rough regime, most studies have used $z_0=k_s/30$ to approximate the surface roughness.

The near-surface wind profile is modified through momentum transfer to saltating particles. Indeed, it is the retardation of the wind profile through drag by saltating particles that ultimately limits the number of particles that can be saltating under given conditions.

3.5 Saltation to steady state

After the saltation fluid threshold has been exceeded, particles lifted from the surface are quickly accelerated by the wind into ballistic trajectories and, after several hops, can have gathered sufficient momentum to splash surface particles. These newly ejected particles are themselves accelerated by wind and eject more particles when impacting the surface, causing an exponential increase in the horizontal saltation flux in the initial stages of saltation. This rapid increase in the particle concentration produces a corresponding increase in the drag of saltating particles on the fluid, thereby retarding the wind speed. This in turn reduces the speed of saltating particles, such that a steady state is reached when the speed of saltating particles is reduced to a value at which there is a single particle leaving the soil surface for each particle impacting it.

The distance required for saltation to reach steady state is characterized by the saturation length. Its value depends on several length scales in saltation, such as the length of a typical saltation hop, the length needed to accelerate a particle to the fluid speed, and the length required for the drag by saltating particles to retard the wind speed. The saturation distance is about 10 to 30 m for dry loose sand.

In addition to the saturation length, the adjustment distance is another characteristic length scale over which the horizontal saltation flux increases to a steady state. The corresponding adjustment effect arises because the atmospheric boundary layer flow adjusts to the increased roughness of the surface layer produced by saltation. The increased surface roughness acts as a greater sink of horizontal fluid momentum, which increases the downward flux of fluid momentum, thereby increasing the wind shear velocity for a given free stream wind speed in the atmospheric boundary layer. This process acts as a positive feedback on saltation and is termed the Owen effect. Field studies indicate that the adjustment distance for a flat field site is of the order of about 100 to 200 meters (Davidson-Arnott et al., 2007).

Saltation is in steady state when its primary characteristics, such as the horizontal mass flux and the concentration of saltating particles, are approximately constant with time and distance. Since wind speed can undergo substantial turbulent fluctuations, this is rarely true on timescales longer than minutes or often even seconds, causing saltation to be highly intermittent. In fact, a substantial fraction of sand transport occurs in aeolian streamers or sand snakes, which are probably produced by individual eddies of high-speed air. These streamers have typical widths of about 0.2 meters, thereby producing strong variability on short time and length scales.

The particle concentration in transport-limited saltation is in steady state when there is exactly one particle leaving the soil bed for each particle impacting it. An equivalent constraint is that for each saltating particle lost to the soil bed due to failure to rebound upon impact, another particle must be lifted from the soil bed and brought into saltation by either splash or aerodynamic entrainment.

Wind tunnel experiments show that particles are splashed at impact speeds typical of saltation (about 1 m/s for loose sand). Particle entrainment in steady state is dominated by splash, not by direct fluid lifting.

Figures 3.6 and 3.7 show the saltation distance ($L_{\text{saltation}}$) and saltation height for sand grains in the range of 20 to 500 μm based on the work of Bagnold (1941) and Kok et al. (2012).

It is assumed that:

$$L_{\text{saltation}} = 0.001 (u_*)^2 (d_{50})^{-1} \quad (3.4a)$$

$$\delta_{\text{saltation}} = 0.05 L_{\text{saltation}} \quad (3.4b)$$



The maximum saltation height/length of 50 μm -grains is about 1/20 m during storm conditions (BF 9).

Observations in wind tunnels and in nature show that the particle velocity (averaged over the transport layer thickness) is almost insensitive to the external wind velocity above the transport layer and approximately equal to about $10(gd)^{0.5}$ at the sand surface to about $40(gd)^{0.5}$ at the top of the transport layer. This range is approximately equal to 2 to 5 times critical bed shear velocity ($u_p \cong 2 \text{ to } 5 u_{*,cr}$).

Particle concentration is so high that the wind velocity is strongly reduced to a value of the order of $1 (\pm 0.5)$ m/s. An increase of the wind velocity results in an increase of the particle concentration which in turn leads to a decrease of the wind flow speed close to the bed such that the new equilibrium particle velocity remains almost unchanged (Valance et al., 2015).

Above the saltation layer, the particle concentration is much less and the air flow is almost unaffected by the presence of the particle. As a result, the particle velocity above the saltation layer increases with increasing wind velocity (Valance et al., 2015).

Summarizing: the speed of energetic particles moving mostly at the top of the transport layer increases with the bed-shear velocity u_* , whereas the speed of less energetic particles moving mostly close to the sand surface remains approximately constant.

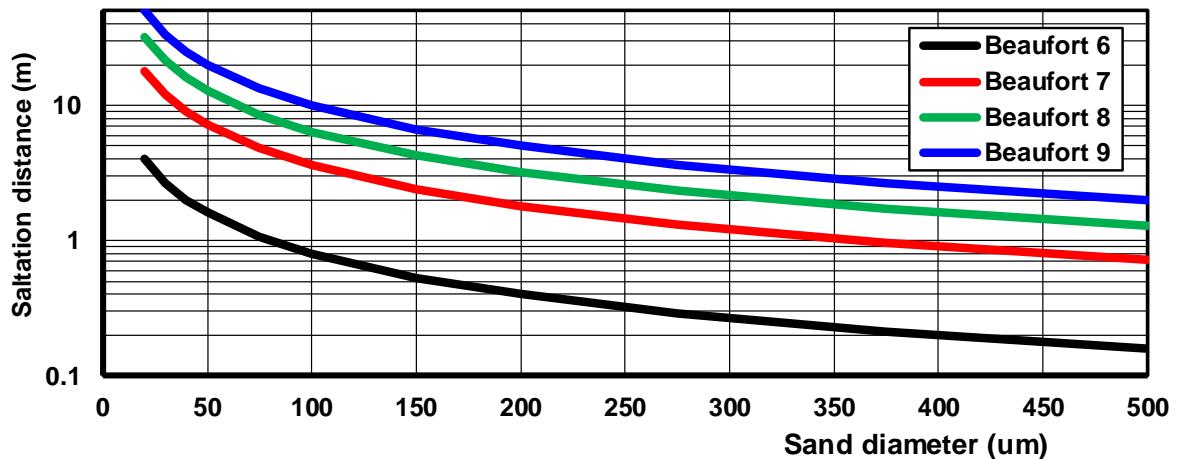


Figure 3.6 Saltation distance as function of sand diameter and wind speed

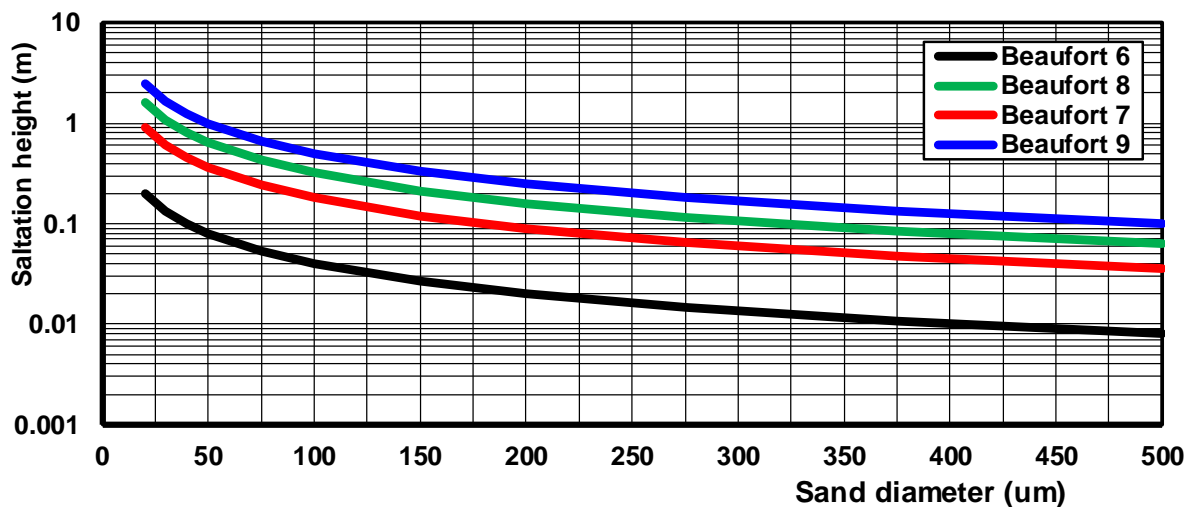


Figure 3.7 Saltation height as function of sand diameter and wind speed

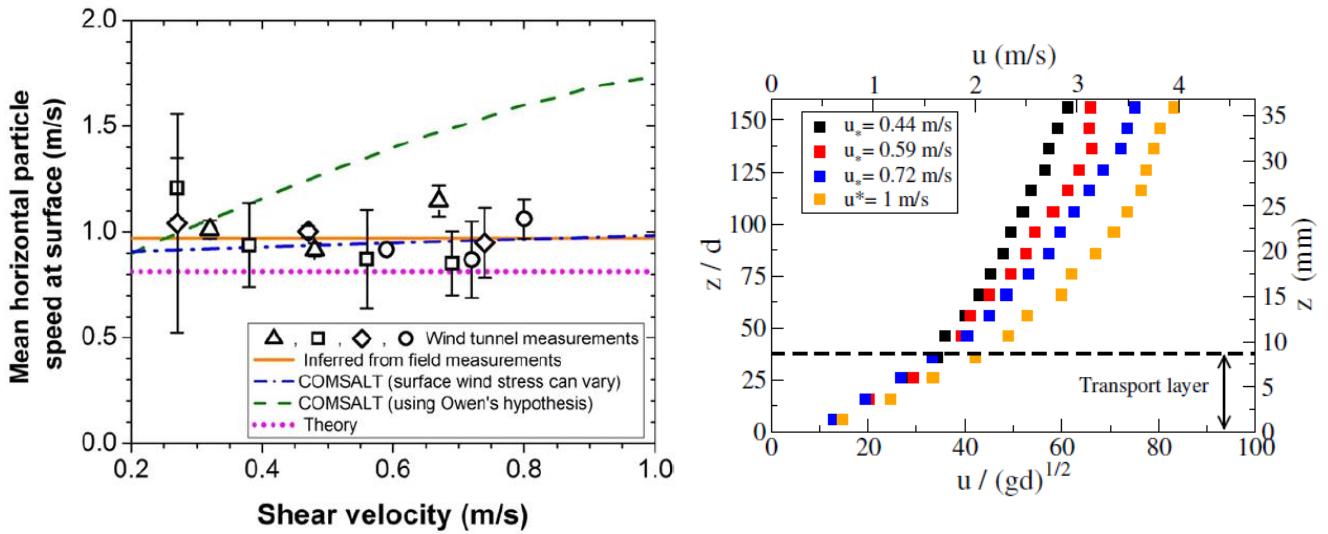


Figure 3.8 Particle velocity data
Left: Measured and computed mean horizontal particle velocity at surface (Kok et al., 2012)
Right: Measured particle velocity profiles for sand $d_{50}=0.23$ mm (Valance et al., 2015)

3.6 Total sediment mass flux in saturated conditions

Sand transport commences as soon as the threshold is exceeded. The dominant mode of transport for sand particles in the size range of 100 to 300 μm is the saltation type of transport (small ballistic type of hops). Very small particles (fine fraction) ranging from 63 to 100 μm are transported in suspension by turbulent eddies. The largest particles (coarse fraction) ranging from 300 to 2000 μm are transported by sliding and rolling as surface creep. The transport of particles by rolling, sliding and small hops (saltations) can be defined as bed load transport of particles in more or less continuous contacts with the bed. Bed load transport of particles in a thin transport layer is the dominant mode of transport for sand particles (100 to 300 μm) in air. Observations in wind tunnels and in nature show that most of the transport occurs in a thin layer (< 0.03 m) above the sand surface (Ho, 2012.). In this thin transport layer, the particle velocity (averaged over the layer thickness) is almost insensitive to the external wind velocity above the transport layer and approximately equal to the 3 to 4 times critical bed shear velocity ($u_p \approx 3$ to $4 u_{*cr}$). Particle concentration is so high that the wind velocity is strongly reduced to a value of the order of 0.8 to 1.2 m/s (Kok et al., 2012). An increase of the wind velocity results in an increase of the particle concentration which in turn leads to a decrease of the wind flow speed close to the bed such that the new equilibrium particle velocity remains almost unchanged (Valance et al., 2015).

Above the saltation layer, the suspended particle concentration is much less and the air flow is almost unaffected by the presence of the particle. As a result, the particle velocity above the saltation layer increases with increasing wind velocity (Valance et al., 2016).

Similar to sand transport in rivers, the sand transport of dry sand in air can be described by a set of dimensionless parameters, being:

- dimensionless transport rate $\phi = q_{s, \text{mass}} / (\rho_s s^{0.5} g^{0.5} d_{50}^{1.5})$;
- dimensionless grain size $D^* = [(s-1) g / \nu^2]^{1/3} d_{50}$;
- dimensionless bed-shear stress $\theta = u_*^2 / [(s-1) g d_{50}]$;
- dimensionless density $s = \rho_s / \rho_a$ and $s-1 \approx s$ for air



with:

- $q_{s,mass}$ = mass sand transport (in kg/m/s);
- ρ_s = sediment density (2650 kg/m³);
- ρ_a = air density (1.2 kg/m³);
- d_{50} = median grain size (m);
- ν = kinematic viscosity of air (1.33 10⁻⁵ m²/s for 0 °C and 1.5 10⁻⁵ m²/s for 20 °C);
- u^* = bed-shear velocity (m/s).

The sand transport equation can be formulated as:

$$\phi = \alpha_1 (D^*)^\beta (\theta - \theta_{cr})^\gamma \quad (3.5)$$

with: α_1, β, γ = coefficients.

Following Bagnold (1941) for bed-load transport in air and Meyer-Peter and Mueller (1948) for bed-load transport in water, $\gamma=1.5$ and thus:

$$q_{s,mass} = \alpha_1 (D^*)^\beta \rho_s [s^{0.5} g^{0.5} d_{50}^{1.5}] [s^{-1.5} g^{-1.5} d_{50}^{-1.5}] [u^{*2} - u_{*,cr}^2]^{1.5}$$

$$q_{s,mass} = \alpha_1 (D^*)^\beta \rho_s s^{-1} g^{-1} [u^{*2} - u_{*,cr}^2]^{1.5}$$

$$q_{s,mass} = \alpha_1 (D^*)^\beta (\rho_a/g) [u^{*2} - u_{*,cr}^2]^{1.5}$$

$$q_{s,mass} = \alpha_2 (D^*)^\beta (\rho_a/g) [u^{*3} - u_{*,cr}^3]$$

$$q_{s,mass} = \alpha_2 [(s g/\nu^2)^{\beta/3} (d_{50,ref})^\beta] (d_{50}/d_{50,ref})^\beta (\rho_a/g) [u^{*3} - u_{*,cr}^3]$$

Using: $s=2650/1.2=2208$, $\nu=1.4 \cdot 10^{-5} \text{ m}^2/\text{s}$, $d_{50,ref}=0.00025 \text{ m}$, $\beta=0.5$, it follows that

$$q_{s,mass} \cong 3.5 \alpha_2 (d_{50}/d_{50,ref})^{0.5} (\rho_a/g) [u^{*3} - u_{*,cr}^3]$$

$$q_{s,mass} \cong \alpha_B (d_{50}/d_{50,ref})^{0.5} (\rho_a/g) [u^{*3} - u_{*,cr}^3]$$

which is a modified Bagnold-equation.

Based on the work of Bagnold: $\alpha_B=3.5\alpha_2 \cong 2$

The modified Bagnold-equation for **dry** sand particles is herein given as:

$$\text{Modified Bagnold (1941):} \quad q_{s, \text{equilibrium}} = \alpha \alpha_B \alpha_{adj} \alpha_{shell} (d_{50}/d_{50,ref})^{0.5} (\rho_{air}/g) [(u^*)^3 - (u_{*,cr}^3)] \quad (3.6)$$

Another expression is

$$\text{Kok et al. (2012):} \quad q_{s, \text{equilibrium}} = \alpha \alpha_{DK} \alpha_{adj} \alpha_{shell} (\rho_{air}/g) u_{*,cr} [(u^*)^2 - (u_{*,cr}^2)] \quad (3.7)$$

$$\text{Critical shear stress Bagnold (1941):} \quad \begin{aligned} u_{*,cr} &= \alpha_{cr} \alpha_{mois} [(\rho_s/\rho_{air}-1) g d_{50}]^{0.5} && \text{for } d_{50} > 100 \mu\text{m} \\ u_{*,cr} &= \alpha_{cr} \alpha_{mois} u_{*,cr,100 \mu\text{m}} && \text{for } 20 < d_{50} < 100 \mu\text{m} \end{aligned} \quad (3.7)$$

$$\text{Shear stress:} \quad u^* = \kappa \alpha_{veg} \alpha_{sh} \alpha_{site} U_{wind10}/\ln(30h_{wind}/k_s) \quad (3.8)$$



with:

- $Q_{s, \text{equilibrium}}$ = mass flux of sediment at equilibrium conditions (saturated transport);
 d_{50} = particle size (m);
 $d_{50, \text{ref}}$ = reference particle size = $250 \cdot 10^{-6}$ m (250 μm);
 ρ_{air} = density of air ($\cong 1.2$ kg/m³);
 g = acceleration of gravity (m/s²);
 u^* = surface shear velocity due to wind forces (m/s);
 $u^*_{, \text{cr}}$ = surface shear velocity at initiation of motion; threshold shear velocity (m/s);
 k_s = equivalent roughness length scale of Nikuradse (m); about 5 to 100 d_{50} for low to high wind velocities over a flat surface (k_s is proportional to thickness of thin transport layer);
 $U_{\text{wind}10}$ = wind velocity at 10 m above the surface (m/s);
 h_{wind} = height at which wind velocity is defined (= 10 m);
 κ = constant of Von Karman (=0.4);
 α = calibration factor (default=1 for natural dry, loose sand particles);
 α_B = Bagnold-coefficient for dry sand
($\cong 1.5$ for uniform sand; $\cong 1.8$ for naturally graded sand; $\cong 2.8$ for widely graded sand);
 α_{DK} = DK-coefficient ($\cong 5$) for natural dry, loose sand particles;
 α_{adj} = adjustment coefficient = $L_{\text{fetch}}/L_{\text{adjustment}}$; (maximum 1);
 α_{shell} = $(1-2p_{\text{shell}}/100)^2$ = reduction coefficient related to the presence of shells;
 α_{cr} = 0.11 based on data of Shao-Lu (2000) and Han et al. (2011); $\cong 0.1$ based on Bagnold (1941);
 α_{mois} = moisture coefficient = $1+2\tanh(mc-0.25)$; $\alpha_{\text{mois}} = 1$ for $mc \leq 0.25\%$ dry sand; based on data of Han et al. (2011); see Section 3.2;
 α_{veg} = vegetation coefficient (none= 1; <1 if vegetation is present);
 α_{sh} = sheltering coefficient ($\alpha_{\text{sh}} < 1$ for sheltered sites; $\alpha_{\text{sh}} = 1$ for exposed sites);
 α_{site} = coefficient for sites higher than the beach (giving higher wind speed) = $1+0.03h_{\text{site}}$;
 mc = moisture content= ratio of mass water and mass dry sand in sample $\times 100\%$;
 p_{shell} = percentage of shells (0 to 30%);
 h_{site} = site level above beach level (m); $h_{\text{site}} = 0$ m for sand transport at beach.
 L_{fetch} = fetch length at beach (input; about 10 to 100 m normal at beach)
 $L_{\text{adjustment}}$ = adjustment length scale of sand transport to equilibrium transport (input; about 100-200 m).

Example computations

In the case of dry sand with $d_{50} = 300 \mu\text{m} = 0.0003$ m; $u^*_{, \text{cr}} = 0.28$ m/s; $\alpha_{\text{cr}} = 0.11$; $\alpha = 1$, the computed sand transport is as follows:

$$u^* = 0.5 \text{ m/s: } Q_{s, \text{equilibrium, Bagnold}} = 2 \times (300/300)^{0.5} (1.2/9.81) (0.5^3 - 0.28^3) = 0.025 \text{ kg/m/s}$$

$$Q_{s, \text{equilibrium, DK}} = 5 \times (1.2/9.81) \times 0.28 \times (0.5^2 - 0.28^2) = 0.029 \text{ kg/m/s}$$

$$u^* = 1.0 \text{ m/s: } Q_{s, \text{equilibrium, Bagnold}} = 2 \times (300/300)^{0.5} (1.2/9.81) (1^3 - 0.255^3) = 0.24 \text{ kg/m/s}$$

$$Q_{s, \text{equilibrium, DK}} = 5 \times (1.2/9.81) \times 0.28 \times (1^2 - 0.28^2) = 0.16 \text{ kg/m/s}$$

$$u^* = 2.0 \text{ m/s: } Q_{s, \text{equilibrium, Bagnold}} = 2 \times (300/300)^{0.5} (1.2/9.81) (2^3 - 0.255^3) = 1.95 \text{ kg/m/s}$$

$$Q_{s, \text{equilibrium, DK}} = 5 \times (1.2/9.81) \times 0.28 \times (2^2 - 0.28^2) = 0.67 \text{ kg/m/s}$$



Figure 3.9 shows the wind-induced sand transport of dry, loose sand based on the formula of Bagnold for three sand diameters. It can be seen that the wind transport increases with grain diameter for wind speeds > 12 m/s (factor $d_{50}^{0.5}$ is dominant) and decreases with grain diameter for wind speeds < 12 m/s ($u_{*,cr}$ is dominant).

The effect of vegetation is also shown for particles of 300 μm . It is assumed that: $\alpha_{veg}=0.75$ for minor vegetation with about 5 grass plants per m^2 and $\alpha_{veg}= 0.5$ for major vegetation with about 15 grass plants per m^2 . Major vegetation strongly reduces the sand transport capacity.

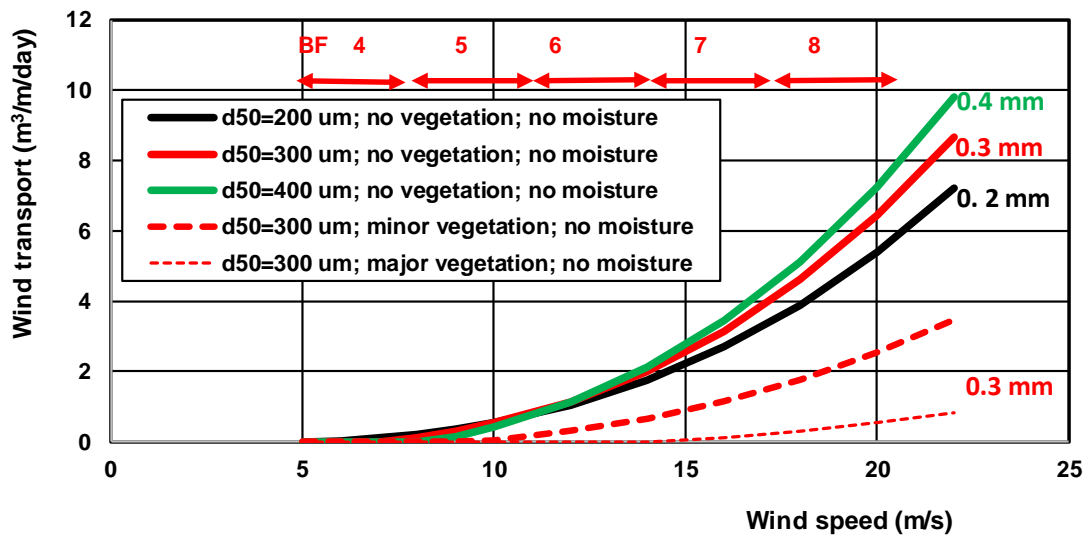


Figure 3.9 Wind transport of dry, loose sand particles at beach based on Bagnold-equation. ($k_s = 0.01 \text{ m}$, $h_{wind} = 10 \text{ m}$, $\kappa = 0.4$, $\rho_a = 1.2 \text{ kg/m}^3$, $\alpha_B = 2$; $L_{fetch} = L_{adjustment} = 100 \text{ m}$; $\alpha = 1$; $\alpha_B = 2$; $\alpha_{DK} = 5$)

Wind tunnel experiments China

Han et al. (2011) studied the effect of moisture content on sand transport by wind in a wind tunnel (length=37m, width=1.2m, height=1.2 m) in China, see Figure 3.10. Sand trap measurements were done at the end of a sand tray with length of 4 m. The bed consisted of sand with $d_{50}=0.203 \text{ mm}$. The sand trap (efficiency of 90% for particles >0.1 mm) had a height of 0.6 m and was sectionalized in 60 openings with height of 10 mm and width of 5 mm. The lowest opening is flush with the sand surface. The wind velocity was measured at $z=0.6 \text{ m}$ above the flat sand surface using a Pitot-tube method. The moisture content (ratio of mass of water and mass of dry sand $\times 100\%$) of the sand bed was varied in the range of 0.14% to 2.7%. The moisture content of the sand bed was prepared just before the experiment using distilled water. Each experiment was run over only 90 s to prevent a change of the moisture content. Five bed surface samples were taken after each experiment to determine the moisture content again.

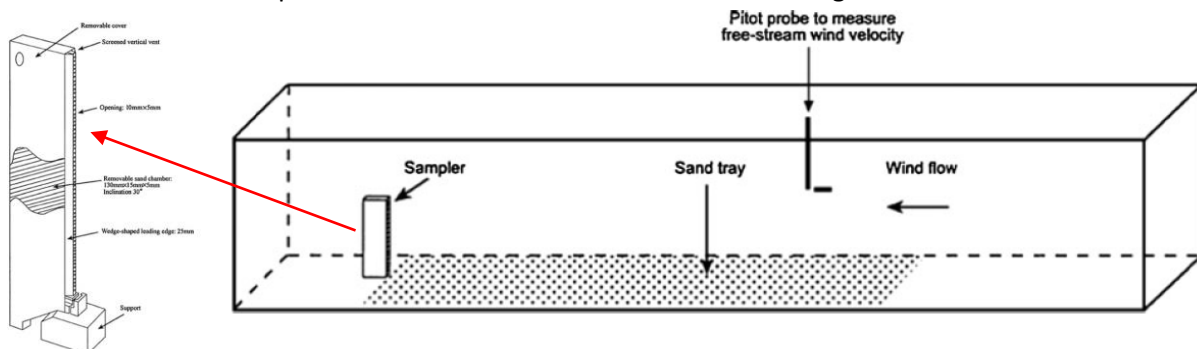


Figure 3.10 Experimental setup in wind tunnel and sand trap sampler (Han et al. 2011)



Wind velocity at 0.6 m above sand surface (m/s)	Sand transport for dry sand bed (kg/m/s)		
	Measured	Computed Bagnold model ($\alpha_B=2$; $\alpha_{cr}=0.11$; $k_s=5$ mm)	Computed DK-model ($\alpha_{DK}=5$; $\alpha_{cr}=0.11$; $k_s=5$ mm)
10	0.02	0.023	0.026
12	0.07	0.042	0.041
14	0.14	0.068	0.058
16	0.25	0.10	0.079
18	0.38	0.15	0.101
20	0.60	0.20	0.127

Table 3.3 Comparison of measured and computed depth-integrated sand transport; dry sand $d_{50}=0.203$ mm (moisture content <0.25%)

Wind velocity at 0.6 m above sand surface (m/s)	Sand transport for dry sand bed (kg/m/s)					
	Measured			Computed Bagnold model ($\alpha_B=2$; $\alpha_{cr}=0.11$; $k_s=5$ mm)		
	mc=1%	mc=2%	mc=2.7%	mc=1%	mc=2%	mc=2.7%
10	0.035	0.033	0.018	0.	0.0	0.
12	0.10	0.042	0.019	0.013	0.0	0.
14	0.17	0.045	0.025	0.039	0.006	0.
16	0.23	0.056	0.025	0.074	0.04	0.034
18	0.27	0.052	0.02	0.12	0.085	0.078
20	0.31	0.057	0.019	0.17	0.14	0.13

Table 3.4 Comparison of measured and computed depth-integrated sand transport; moisture sand $d_{50}=0.203$ mm (moisture content 1% to 2.7%)

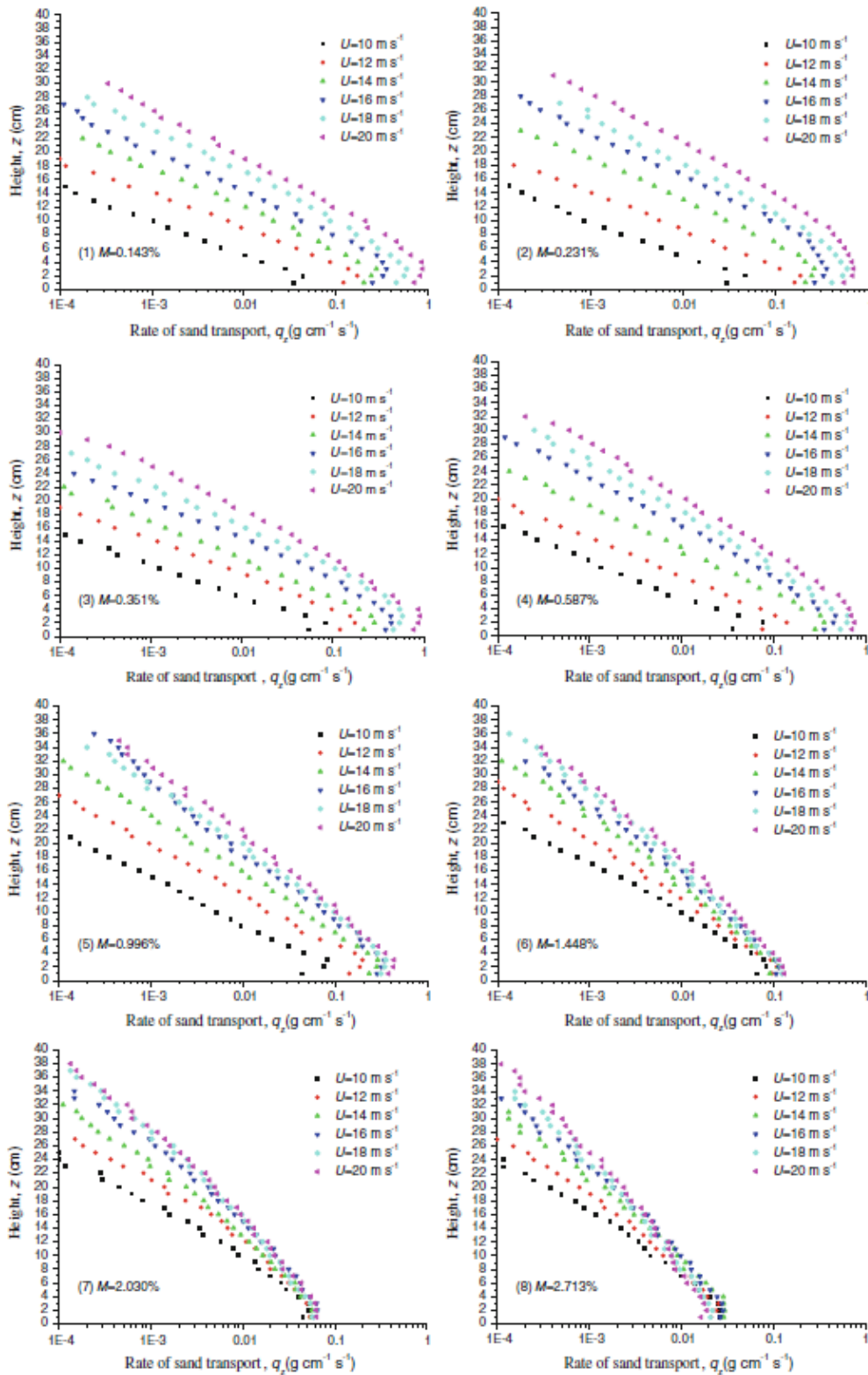


Figure 3.11 Sand flux profiles for various moisture contents and wind velocities (sand flux in gram/cm²/s; height in cm); (Han et al. 2011)

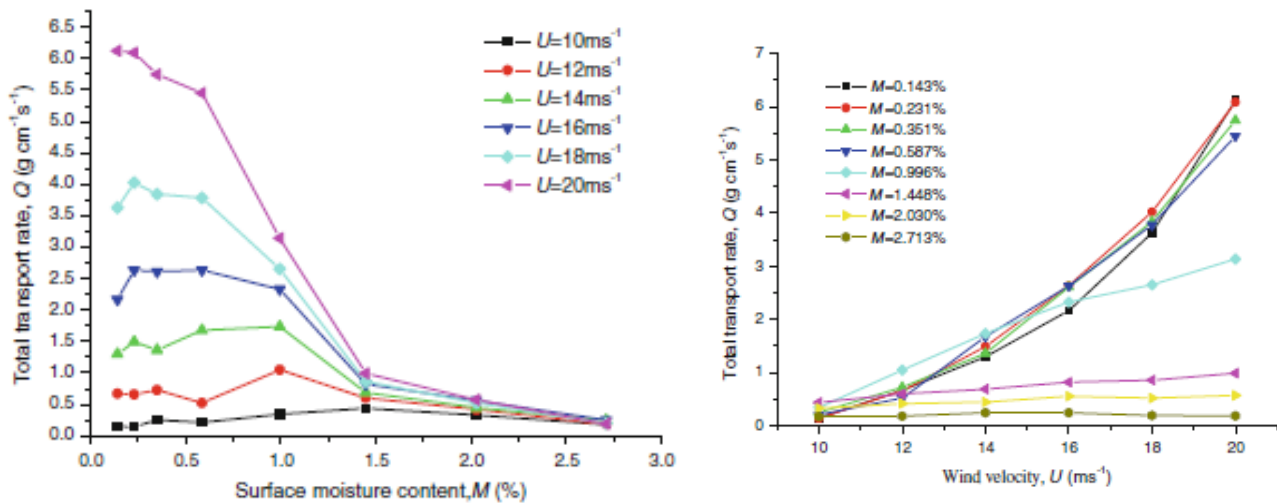


Figure 3.12 Depth-integrated sand transport as function of wind velocity and moisture content (Han et al., 2011)

Field experiment southeastern part of Tengger desert in China

Dong et al. (2012) performed a field experiment in desert conditions. This area is a typical shifting dune field free of any vegetation and dominated by dunes. The primary ridges of the dunes are 3 to 20 m tall, spaced at 30 to 170 m, and aligned in a NE-SW direction. The subsidiary ridges are 1 to 6 m tall, spaced at 20 to 70 m, and aligned in a NW-SE direction. Annual precipitation is about 180 mm, most of which falls in the summer and autumn. An area of 600 x 800 m² was flattened to permit observations of aeolian transport (2005). Three plots of 80x80 m² were established within the area (**Figure 3.13**):

- an area of open shifting sand was flattened without further treatment to ensure that sediment transport came from both outside and inside the plot;
- an enclosed plot of shifting sand was surrounded by 20 m wide straw checkerboard barriers on all four sides to ensure that sediment transport came primarily from inside the plot;
- a gravel-covered plot was established by creating a 30-mm-thick layer of gravel with a mean diameter of 3 mm that completely covered the sand surface to ensure that sediment transport came exclusively from outside the plot.

The three plots (dry sand with $d_{50}=0.19$ mm) were aligned perpendicular to the primary NW wind.

Wind data (free-stream wind velocity) was acquired from a meteorological tower at the center of the site at eight heights (1, 2, 4, 8, 16, 24, 32, and 48 m above the surface) using wind sensors connected to a data logger. The wind data acquisition system was set to record wind velocity averaged at 1-min intervals. The aeolian transport observation plots were 100 to 300 m upwind from the central meteorological tower.

Sediment transport was measured in April and May 2008 using vertical segmented sediment samplers (LDDSEG samplers) designed by the Key Laboratory of Desert and Desertification, Chinese Academy of Sciences. This sampler is about 1 m tall and is divided into 50 openings (each 20 mm \times 20 mm) to collect the horizontally transported wind-eroded sediment at 50 heights at 20-mm intervals. Each opening is connected to a sediment chamber that is inclined downward at an angle of 30° with respect to the horizontal, and the chamber is removed after each observation period. The sampler was evaluated in a wind tunnel before using it at the study site. Sampling efficiency of the samplers defined in wind tunnel tests for dune sand from this area ranged from 72 to 87%. An overall sampling efficiency of 80% (the average sampling efficiency) was adopted in the present study to correct the transport data. Simultaneous sediment transport observations were conducted in the three plots using one LDDSEG sampler per plot, installed at the downwind edge of



each plot. **Table 3.5** shows 5 characteristic data of the measured sand transport data of Dong et al. (2012) for the open sand plot. The variability of the measured data is relatively large (factor 2 to 3 for each wind velocity class) due to wind velocity fluctuations. The measured transport rates of the enclosed sand plot were

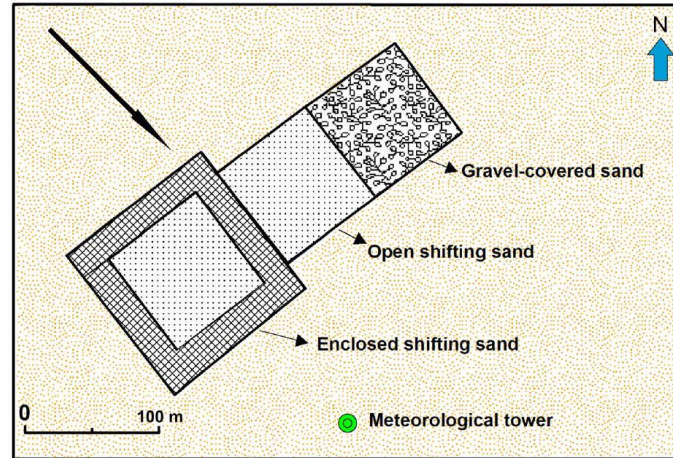


Figure 3.13 Experimental setup (Dong et al., 2012)

The plot with enclosed shifting sand and the gravel-covered plot had similar transport rates that were lower (factor 2) than that above the plot with open shifting sand. These differences suggest that sediment availability is an important factor in determining the transport rate. Given the horizontal dimension of about 80 m, the adjustment length scale for dry sand is of the order of 100 to 150 m.

Flux density profiles above all three plots were expressed well by an exponential decay function to describe the saltation flux density profiles.

The computed transport rates of the Bagnold-equation and the DK-equation are much too small (factor 3), see **Table 3.5**.

Wind velocity at 16 m above the sand surface (m/s)	Effective thickness of sand transport layer (m)	Measured sand transport		Computed sand transport	
		(kg/m/hour)	(kg/m/s)	Bagnold $\alpha_B=2$ (kg/m/s)	DK $\alpha_{DK}=5$ (kg/m/s)
5.5 (± 0.5)	0.25	2	0.00055	0.	0.
6.5 (± 0.5)	0.3	5	0.0014	0.00011	0.00021
7.5 (± 0.5)	0.35	15	0.0042	0.0014	0.0025
8.5 (± 0.5)	0.4	30	0.0083	0.0032	0.0052
10 (± 0.5)	0.5	70	0.019	0.0067	0.0097

Table 3.5 Measured sand transport events; plot open shifting sand; dry sand $d_{50}=0.19$ mm



Field experiment Texel beach 2013, The Netherlands

A small-scale field experiment was done by the author at the beach of Texel (The Netherlands) in July 2013; beach sand of about 0.2 to 0.25 mm (dry, loose particles). A strong wind was blowing parallel to the water line at a wind speed of about $U_{wind10} = 8$ to 10 m/s (Beaufort 5 to 6).

The beach particles were moving by sliding, rolling and saltating in a thin layer of 2 to 3 mm thick with a speed of about 0.2 to 0.4 m/s (carpet-type of transport). About 10% of the surface was moving and wind gusts were very important resulting in intermittent transport processes.

Small-scale ripples were present (height of 0.01 to 0.03 m, length of 0.2 to 0.3 m).

A small trench (length=0.1 m; width=0.1 m) was made normal to the wind. The trench was completely filled in about 30 minutes yielding a transport rate of about $q_s = 0.01$ kg/m/s (bulk density of 1600 kg/m³).

Using: $\alpha_{cr}=1$; $\alpha_B=2$; $\alpha_{DK}=5$; $d_{50}=0.225$ mm, $k_s=0.03$ m, $U_{wind10}=9$ m/s, yields:

$$u_{*,cr} = 0.282 \text{ m/s}, u_* = 0.39 \text{ m/s};$$

$$q_{s,bagnold} = 2 \times (0.225/0.3)^{0.5} \times (1.2/9.81) \times [0.39^3 - 0.242^3] = 0.010 \text{ kg/m/s}$$

$$q_{s,dekok} = 5 \times (1.2/9.81) \times 0.242 \times [0.39^2 - 0.242^2] = 0.014 \text{ kg/m/s}$$

Both values are in good agreement to the measured value of 0.01 kg/m/s.

Field experiment Koksijde beach 2013, Belgium

A field experiment was done by Campos (2018) at the beach of Koksijde in Belgium. The measurement location was the dry beach outside the wet intertidal beach zone. The beach sand has a $d_{50}=0.22$ mm. Wind-induced sand transport was measured by using 6 streamer type traps on top of each other (**Figure 3.14**). Each trap has a length of 25 cm; an opening with vertical size of 5 cm; horizontal size of 10 cm. The sand particles are trapped in a nylon bag (length of 50 cm to 75 cm for the lowest trap) with mesh size of 50 μ m. The sand trap data are presented in **Table 3.6**. The mass of sand in the lowest trap varies between 6% and 75% of the total mass. Hence, about 70% of the sand transport occurs in the lowest 5 cm of the transport layer. The sand transport is computed as the total trap mass divided by the duration and the mouth width (=0.1 m). The data can be summarized into three different cases (see **Table 3.7**). Computed values of the Bagnold-equation and the DK-equation are somewhat too small (factor 1.5 to 2).

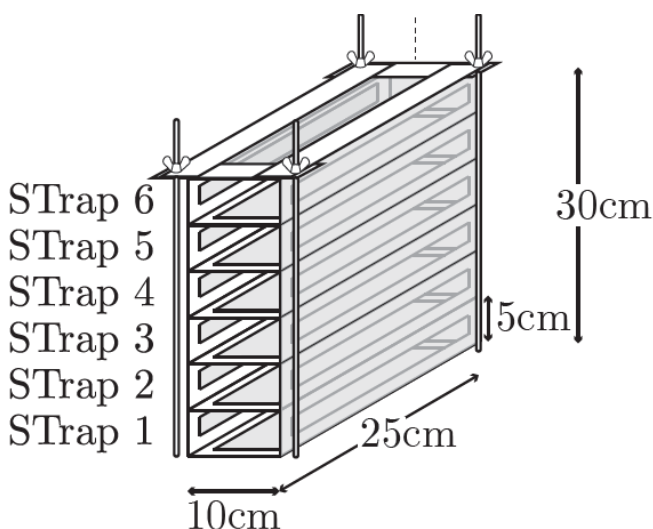


Figure 3.14 Streamer type sand traps (Campos, 2018)



Wind velocity at 0.5 m above surface	Duration of event (s)	Sand transport trapped (in grams)							Sand transport (kg/m/s)
		Trap 1 0-5 cm	Trap 2 5-10 cm	Trap 3 10-15 cm	Trap 4 15-20 cm	Trap 5 20-25 cm	Trap 6 25-30 cm	Total	
7.2	2200	1968	655	145	50	14	5	2826	0.013
8.4	960	1498	448	133	45	17	9	2150	0.022
8.7	1050	1508	560	169	61	26	13	2337	0.022
9.2	1440	2938	907	301	106	45	22	4319	0.03
9.2	1080	2178	693	226	92	39	18	3246	0.03
9.1	1440	2687	605	186	68	30	16	3592	0.025
9.2	1320	2439	730	248	101	45	20	3583	0.027
9.2	2250	3529	1045	352	140	61	32	5159	0.023

Table 3.6 Sand trap data Koksijde beach, Belgium (Campos, 2018)

Wind velocity at 0.5 m above the sand surface (m/s)	Effective thickness of sand transport layer (m)	Measured sand transport (kg/m/s)	Computed sand transport ($k_s=5$ mm)	
			Bagnold $\alpha_B=2$ (kg/m/s)	DK $\alpha_{DK}=5$ (kg/m/s)
7.2 (± 0.3)	0.3	0.013	0.007	0.01
8.5 (± 0.3)	0.3	0.022	0.013	0.017
9.2 (± 0.3)	0.3	0.026	0.018	0.021

Table 3.7 Measured and computed sand transport; dry sand $d_{50}=0.22$ mm; Koksijde beach Belgium

3.7 Processes affecting sediment transport

Wind speed acceleration

Wind normal to the beach accelerates along the slope of the foredune and is maximum at the dune crest level.

The influence of topography on wind speed is prominent (Arens et al., 1995). The maximum speed-up increases with height of the foredune. An increase in height from the beach to the dune crest of about 10 m causes an increase in windspeed of about 20% to 40% (see α_{site} -coefficient of Equation 3.8) in the case that the wind speed is measured at the beach (reference value). This will result in an increase of the sand-carrying capacity. A further increase in foredune height > 10 m appears to have limited influence, probably because the increase in height (acceleration) is compensated by an increase in roughness due to the presence of irregularities at the dune crest.

Figure 3.15 shows the computed aeolian wind transport at the beach level and at various dune crest levels for sand of $300 \mu\text{m}$. The aeolian sand transport increases gradually with increasing crest level as the wind speed increases gradually at higher crest levels due to acceleration effects along the slope of the foredune. The sand transport at a dune crest of 10 m above the beach is about twice (factor of 2) the sand transport at the beach.

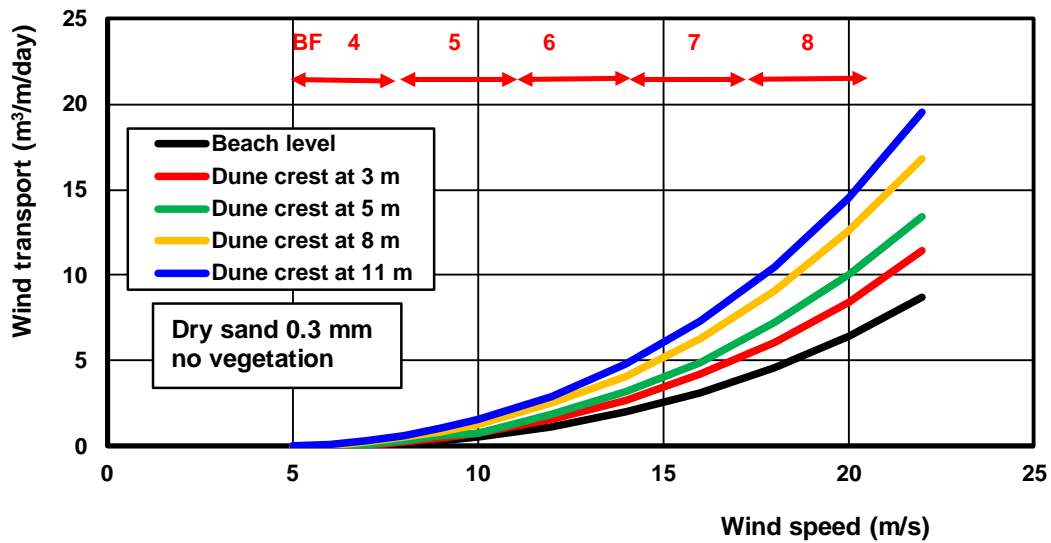


Figure 3.15 Aeolian sand transport at beach level and at various dune crest levels; $d_{50} = 300 \mu\text{m}$; wind speed at 10 m above the beach level

Adjustment length scale

Transport conditions (u^* and u^*_{cr}) vary in time and space due to variations of environmental parameters. As a result, the actual sediment transport rate will often differ from the equilibrium (potential) transport rate. When transport conditions change, the transport rate adjusts/adapts to the new conditions within a certain time span and within a certain distance. Time and distance are related to each other through the velocity of the saltating grains. Wind tunnel and modelling research on dry, loose sand surfaces has shown that equilibrium transport typically is reached in a few seconds (say 10 s). During saltation, the average horizontal velocity of the grains may be of the order of 3 to 10 m/s. A spatial change in transport conditions may cause changing mass fluxes over a distance of about 10 m for dry, loose sand. The distance over which the sediment transport adjust to new equilibrium conditions is known as the adjustment length scale (L_{ad}) and depends on the particle size and wind speed. The L_{ad} -value is smaller for depositing conditions than for eroding conditions.

The field work of Davidson-Arnott et al. (2007) at a Canadian beach with sand of 0.26 mm shows an adjustment length (the distance at which the transport reaches a maximum) of about 100 to 200 m for the combination of measured wind speeds and moisture contents. Similar length scales (100 to 200 m) can be derived from the work of Dong et al. (2012). The adjustment length associated with each event is defined as the distance along the beach from the upwind boundary, defined by either the vegetation line for offshore-directed winds (from land to sea), or the zone of high moisture content (about 8%) associated with the swash line for onshore-directed winds (from sea to land).

It is not clear whether the maximum transport rate with moist sand is always less than that for dry sand, see Figure 3.16. Relatively high transport rates were measured in conditions with offshore winds when sand supplied from the dry upper beach was transported over a damp, hard surface on the lower foreshore. These high transport rates are probably a reflection of the lower momentum losses for sand impacts with the hard surface.

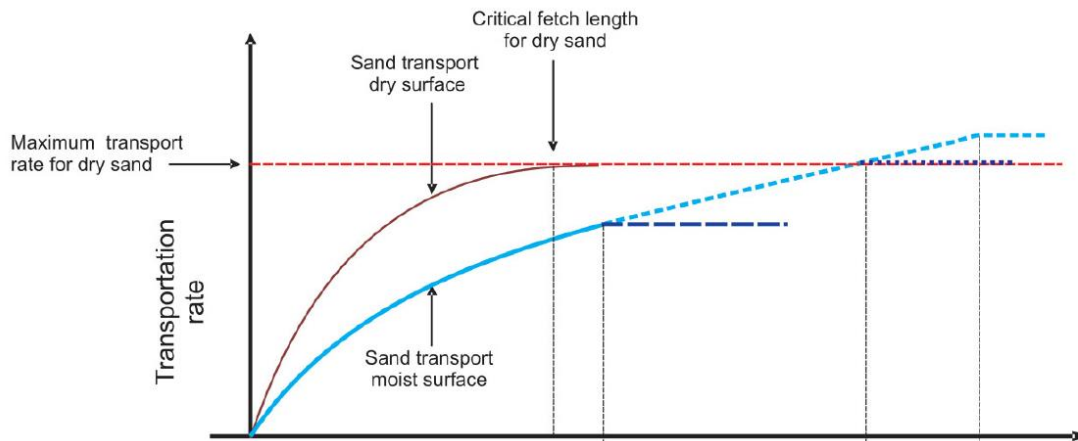


Figure 3.16 Sketch of adjustment length scale for dry and moist sand (Davidson-Arnott et al. 2007)

Where surface moisture is quite high, there is the chance that some saltating grains will adhere to the surface on impact and thus be taken out of the saltation cascade. Where bedforms such as ripples or low barchan dunes are present, grains resting on the surface for more than a few seconds in the lee of the bedform tend to become wet due to capillarity processes and are only dislodged from the stoss slope by impact of saltating grains from upwind. In these conditions it might be expected that the transport rate will never equal that for dry sand. If surface moisture is lower, sufficient dry sand may accumulate where the fetch is long enough (e.g. for highly oblique winds) that the transport rate will eventually equal that for dry sand.

Finally, the transport rate may exceed that for dry sand if the sand supply comes from a dry upwind zone and the sand particles are transported over a moist and hardpacked surface (downwind of the dry surface zone) so that energy loss during collisions with the bed is less than that for a loose, dry sand surface.

The adjustment coefficient can be roughly represented by Equations (3.8) to (3.10).

Modelling of sand transport and sediment transport thus requires not only an ability to predict the wind flow over the sand surface but also, for moist sand, an ability to predict the controls on ejection of grains from the surface and the nature of the rebounds.

Sediment transport in non-saturated conditions

Sediment transport q_s in non-saturated (under-saturated) conditions can be represented as (Van Dijk et al. 1999):

$$q_s = \alpha_{adj} q_{s, equilibrium} \quad (3.9)$$

$$\text{Shear stress: } u_* = \alpha_{veg} \alpha_{sh} K U_{wind10} / \ln(30h_{wind}/k_s) \quad (3.10)$$

$$\text{Critical shear stress: } u_{*,cr} = \alpha_{cr} \alpha_{mois} [(\rho_s/\rho_{air}-1) g d_{50}]^{0.5} \quad (3.11)$$

with:

α_{sh} = sheltering coefficient= 1 for exposed sites; <1 for sheltered sites; =0.8 for beaches under offshore winds;

α_{adj} = adjustment length scale coefficient= $(L_{fetch}/L_{ad})^{0.5}$ with $\alpha_{ad} = 1$ for $L_{fetch} > L_{ad}$;

α_{veg} = vegetation coefficient (< 1); $\alpha_{veg} = 1$ for a flat surface without vegetation;

$\alpha_{veg} = 0.75$ for plants of 0.1 m high and 5 per m^2 (minor vegetation);

$\alpha_{veg} = 0.5$ for plants of 0.2 m high and 15 per m^2 (major vegetation);

α_{mois} = moisture coefficient (> 1); $\alpha_{mois} = 1 + 2 \tanh\{2(mc - 0.25)\}$ and $\alpha_{mois} = 1$ for $mc \leq 0.25\%$

L_{fetch} = available fetch length (normal or parallel to shore/dunes/water line);

$L_{adjustment}$ = adjustment length (100 to 200 m).



Sand dunes and ripples

A flat sand bed exposed to a wind strong enough to set grains into motion is unstable. That is, saltation over an initially flat sand bed results in the generation of two kinds of bedforms with distinct length scales: ripples with length scales of up to $1000d_{50}$ and dunes, which are typically 5 to 10 meters high but can reach heights of a hundred meters. Dunes occur frequently as isolated objects moving on a firm ground (such as barchan dunes in a corridor) but also as part of compounds evolving on a dense sand bed. Ripples appear most commonly on the surface of dunes as chains of small undulations that orient transversely to the wind trend. The physics governing the formation of ripples and dunes has been studied since the pioneering field works by Bagnold (1941, 1954). Many insights have been gained during the last few decades from computer modeling.

3.8 Dust transport

Erosion and emission of dust

Soils without vegetation and low moisture content and consisting of fine sediments are most sensitive to wind erosion and dust emission. The most substantial sources of fine dust-type sediments are deserts and dry lake beds (Kok et al., 2012). A dust storm is the result of strong turbulent winds entraining large quantities of dust particles, reducing visibility.

Very fine (dust-type) particles that can be transported thousands of kilometers from their source regions predominantly have diameters smaller than $20 \mu\text{m}$ (Kok et al., 2012). Dust particles in soils occurs mostly as:

- coatings on larger sand particles;
- part of soil aggregates with a typical size in the range of 20 to $300 \mu\text{m}$.

Dust particles are emitted naturally through three distinct processes (Kok et al., 2012)

- direct aerodynamic lifting;
- ejection of dust from soil aggregates by impacting saltating particles (rupturing the bonds between individual constituents of the aggregates);
- ejection of dust from soil aggregates that are participating in saltation.

The emission of dust-type sediments from either soil aggregates or saltating dust aggregates is thus initiated by wind speeds exceeding the fluid threshold for saltation. Direct aerodynamic lifting of dust requires wind speeds somewhat larger than the saltation threshold (see **Figure 3.2**). Consequently, direct aerodynamic lifting is a less important source of dust than impact-induced emission from dust aggregates in the soil or in saltation. Dust can also be emitted through human activities.

Since dust emission is primarily due to saltation bombardment and subsequent sandblasting, the threshold wind speed above which dust emission occurs is about equal to the saltation threshold. Factors increasing the threshold velocity are cohesive (moisture) effects and hiding effects (fines sediments in between larger roughness elements such as pebbles and stones). The presence of larger roughness elements reduces the wind shear stress on the intervening bare soil and increases the total threshold wind stress required to initiate saltation and dust emission.

The presence of soil moisture can create substantial interparticle forces that inhibit the initiation of saltation, especially for sandy soils. For low relative humidities (below 65%), these interparticle forces are produced primarily by bonding of adjacent adsorbed water layers (hygroscopic forces), whereas for high relative humidities (above 65%) this occurs primarily through the formation of water wedges around points of contact (capillary forces). Water adsorption is governed by electrostatic interactions of the mineral surface with the water molecules. Since sandy soils generally contain a lower density of net electric charges, substantially less water can be adsorbed onto sandy soils than onto clayey soils. Consequently, water bridges form in sandy soils at a relatively low soil moisture content, thereby producing substantial capillary forces.



Often, the vertical dust flux is related to the horizontal saltation flux, as follows: $E_{\text{dust}} = \alpha q_s$, with: α = dust emission efficiency factor in the range of 0.01 to 0.0001, q_s = equilibrium sand transport rate.

The α -coefficient strongly depends on soil properties such as the clay content, the bonding strength of soil dust aggregates, the dry aggregate size distribution and the presence of soil crusts.

Deposition of dust

After emission, mineral dust particles are removed from the atmosphere by either dry deposition or wet deposition. Dry deposition is due to the combined action of gravitational settling with turbulent diffusion in the atmospheric boundary layer and molecular diffusion in the laminar sublayer near surfaces, such as vegetation canopies. Wet deposition includes both in-cloud scavenging, in which dust serve as cloud condensation or ice nuclei and subsequently precipitate, and below-cloud scavenging, in which precipitating raindrops collect dust aerosols. Wet deposition generally dominates for aerosols smaller than about 5 μm in diameter, whereas dry deposition dominates for aerosols larger than about 5 μm . The resulting lifetime of a dust particle decreases with its size and ranges from about 1 to 2 weeks for clay particles (with diameter <2 μm), to several hours or days for silt particles (>2 μm). Consequently, only dust particles smaller than about 20 μm in diameter remain suspended in the atmosphere for sufficient time periods to substantially affect weather and climate.



4. Wind-blown sand transport on beaches

Erosive coasts

The primary dune row is continuously eroded and sand is available for aeolian transport in the downwind direction. Sand is blown into the dune field behind the primary dune row which may result in white dunes (sand covering vegetation). Transgressive dunes can be formed moving landwards. Sand dunes are generally highest and without much vegetation along erosive coasts bordering tidal inlets.

Accretive coasts

The supply of sand is so large that a large buffer of sand is present in front of the primary dune row (wide beach plains) resulting in the generation of new embryonal dunes, dune growth and seaward migration of dunes. Vegetation can generally keep up with aeolian transport.

Stabile coasts

New dunes may be generated at the dune toe and in the upper beach zone. Periodic storm erosion by high tides in combination with wind surges can remove the young dunes after which the cycle is repeated. Vegetation can survive as the aeolian transport is not high enough. The height of the primary dune row may grow slowly.

Annual aeolian sand transport along Holland coast

Based on analysis of sounding data, the net annual aeolian transport at the Holland coast between Hoek van Holland and Den Helder (distance of 110 km) is about 2 to 4 m³/m/year in landward direction across the crest of the primary dune row (De Ruig, 1989).

Arens (2009) has studied the effect of beach nourishment on dune growth. About 55 millions m³ of sand (40% in beach zone and 60% in surf zone) was supplied at the Holland coast (Hoek van Holland-Den Helder; 110 km; The Netherlands) between 1997 and 2007. The dune growth volume was found to be about 22% (12 million m³) of the total beach nourishment volume, which is equivalent with an annual dune volume growth of about 10 m³/m/year.

Example 1

The sand transport equation of Bagnold (1941, 1954) has been used to compute the aeolian transport along a wide beach consisting of dry, loose sand of 0.2 and 0.35mm ($k_s = 0.01$ m, $\rho_s = 2650$ kg/m³, $\alpha_B = 2$, $\alpha_{veg} = 1$, $\alpha_{mois} = 1$, $L_{ad} = 100$ m; $L_{fetch} = 100$ m)

Table 4.1 yields the annual wind transport of sand at a beach with wind from the sectors 180°-210°, 210°-240° en 240°-270° (southwest to northwest). The wind transport (summed over 125 days) is not much affected by particle size.

In practice, the landward transport of sand towards the dune row is a factor of 10 smaller due to moisture and adjustment effects reducing the transport rates (non-saturated transport).

Using: $\alpha_{adj} = 0.5$, $\alpha_{mois} = 1.5$, the windtransport reduces to 13.5 m³/m (normal) and 1.1 m³/m (parallel).



Wind speed (m/s)	Number of days	Wind direction to North	Coast normal to North	Windtransport Bagnold $d_{50}=0.2$ mm (m^3/m)		Windtransport Bagnold $d_{50}=0.35$ mm (m^3/m)	
				normal to shore	parallel to shore	normal to shore	parallel to shore
9 (BF 5)	25	15° (195°)	45°	7.8	-4.5	5.0	-2.9
12 (BF 6)	7	15° (195°)	45°	6.4	-3.7	6.9	-4.0
15 (BF 7)	5	15° (195°)	45°	9.5	-5.5	11.5	-6.6
9	30	45° (225°)	45°	10.8	0	6.9	0
12	10	45° (225°)	45°	10.5	0	11.4	0
15	5	45° (225°)	45°	10.9	0	13.2	0
9	30	75° (255°)	45°	9.4	5.4	6.0	3.5
12	10	75° (255°)	45°	9.1	5.3	9.9	5.7
15	5	75° (255°)	45°	9.5	5.5	11.5	6.6
Totaal	125			84 m³/m	2.5 m³/m	82.4 m³/m	2.3 m³/m

75°=wind direction to which the waves are going; (195°)= wind direction from which the waves are coming

Table 4.1 Windtransport during 125 days of onshore wind

Example 2

A new dune is designed: length= 3 km, width at crest= 40 m; height= 8 m above mean sea level; sand $d_{50}=0.3$ mm; longitudinal dune axis makes an angle of 40 degrees with North (**Figure 4.1**).

The wind rose is divided in 4 quadrants (with respect to the longitudinal axis of the dune, see **Figure 4.1**). Each quadrant has 3 sectors of 30°, as follows:

- Quadrant I (SW-NW): sectors 9, 10, 11; total 120 days
- Quadrant II (NW-NE): sectors 12, 1, 2; total 74 days;
- Quadrant III (NE-SE): sectors 3, 4, 5; total 75 days;
- Quadrant IV (SE-SW): sectors 6, 7, 8; total 97 days;
- All quadrants: total 366 days

Computation results based on AEOLIANTRANSPORT.xls (see Table 4.2)

The computed sand transport rates (in $m^3/m/year$) can be summarized, as:

- wind from quadrants I and IV: transport rates are relatively high (dominant);
- wind from quadrant I (120 days)
normal to SE: 35 $m^3/m/year$ for dry sand decreasing to 1 $m^3/m/year$ for wet sand with vegetation;
parallel to NE: 75 $m^3/m/year$ for dry sand decreasing to 1 $m^3/m/year$ for wet sand with vegetation;
- wind from quadrant IV (97 days):
normal to NW: 26 $m^3/m/year$ for dry sand decreasing to 4 $m^3/m/year$ for wet sand with vegetation;
parallel to NE: 110 $m^3/m/year$ for dry sand decreasing to 20 $m^3/m/year$ for wet sand with vegetation;
- wind from quadrants II and III (149 days): relatively small transport values between 10 and 1 normal to crest;
sand transport decreases significantly (factor 5 to 10) due to presence of vegetation;
- sand transport increases/decreases by 10% for smaller grain diameter (0.25 mm) and larger diameter (0.4 mm);
- based on the computed sand transport rates, the erosion of sand at the dune crest (assumed to be covered with vegetation) is estimated to be about 10 to 15 $m^3/m/year$ at the edges of the dune crest, see **Figure 4.2**.

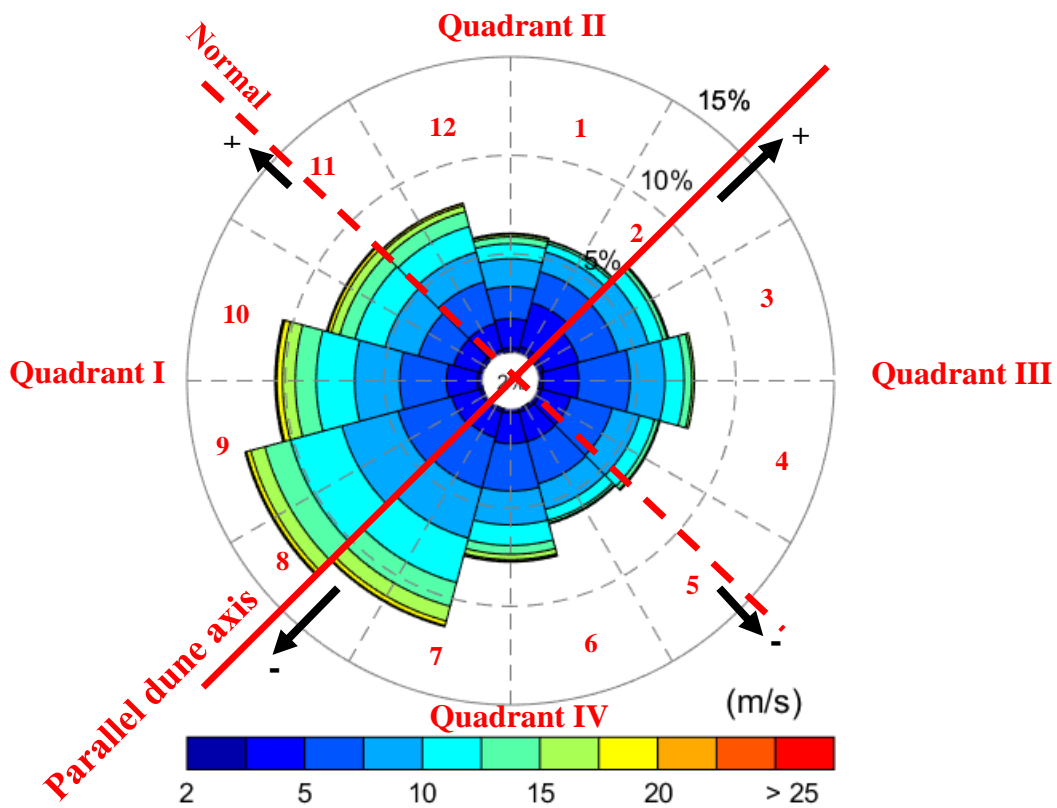


Figure 4.1 Windrose with 4 quadrants and 12 sectors; Sand transport directions (+ or -; black arrows) Parallel dune axis = red line (angle 40° to North); normal to dune axis= dashed red line

Scenarios	Wind transport (m ³ /m/year including pores)									
	Quadrant I ($\alpha_{sh}=0.8$)		Quadrant II ($\alpha_{sh}=0.8$)		Quadrant III ($\alpha_{sh}=1$)		Quadrant IV ($\alpha_{sh}=1$)		All Quadrants	
	nor mal	paral lel	nor mal	paral lel	nor mal	paral lel	nor mal	paral lel	nor mal	paral lel
Dry loose sand, $d_{50}=0.3$ mm No vegetation ($\alpha_{veg}=1$) No moisture ($\alpha_{mois}=1$)	-35	75	-9	-10	11	-37	26	110	-7	138
Wet sand, $d_{50}=0.3$ mm No vegetation ($\alpha_{veg}=1$) Moisture ($\alpha_{mois}=1.3$)	-6	11	-4	-4	6	-20	17	80	13	67
Dry loose sand, $d_{50}=0.3$ mm Vegetation ($\alpha_{veg}=0.8$) No moisture ($\alpha_{mois}=1$)	-4	7	-2	-2	3	-3	9	40	6	42
Wet sand, $d_{50}=0.3$ mm Vegetation ($\alpha_{veg}=0.8$) Moisture ($\alpha_{mois}=1.3$)	-1	1	0	0	1	-3	4	20	4	18

$\rho_{air}=1.2$ kg/m³; $\rho_{sand}=2650$ kg/m³;

Dry bulk density sand = 1600 kg/m³; adjustment length sand transport = 100 m; surface roughness $k_s=0.01$ m

α_{veg} = vegetation coefficient; α_{mois} = moisture coefficient; α_{sh} = sheltering coefficient (reduced wind)

Normal: - = sand transport normal to dune crest in direction south-east; + = in direction north-west

Parallel: - = sand transport parallel to dune crest in direction south-west; + = in direction north-east

Table 4.2 Windtransport at sand dune

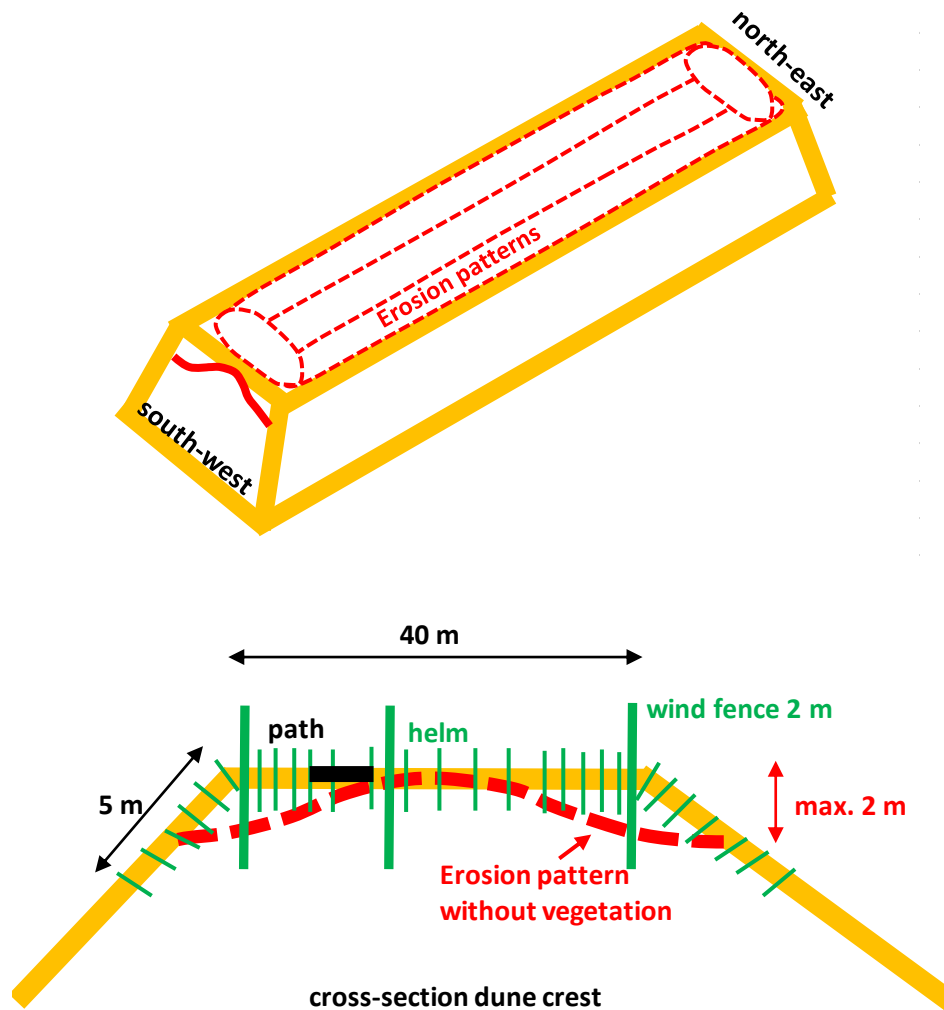


Figure 4.2 Winderosion at dune crest and preventive measures (vegetation and wind fences)

5. Preventive measures to reduce erosion

Erosion due to wind can be reduced to less than $5 \text{ m}^3/\text{m}/\text{year}$ by taking the following measures:

- grass-type vegetation (spinifex; 9 to 10 plants per m^2);
- temporary wind screens/fences (brushwood; lengths of 2 to 2.5 m);
- paper pulp can be sprayed (thin layer) on dry loose sand to reduce erosion (temporary) at dune surfaces without vegetation.

The most effective measure is to plant grass-type vegetation. Usually, it is sufficient to use about 10 plants per m^2 . The plants are manually pushed into small holes made in the dry sand. A team of 5 to 10 men can make a production of about 5000 m^2 per day. Machinery (tractors) can be used at flat surfaces. Planting is done in seasons with some rain, as the plants need some water for growth. After a few years the root system of the plants is penetrated into the sand body over a length of 1 to 3 m.



6. References

- Arens, 2009.** Effecten van suppleties op duinontwikkeling. Rapport 2009.02, Amsterdam
- Arens, S.M., Van kaam-Peters, H.M.E. and Van Boxel, J.H., 1995.** Air flow over foredunes and implications for sand transport. *Earth Surface Processes and Landforms*, Vol. 20, 315-332
- Bagnold, R.A. 1941, 1954.** The physics of blown sand and desert dunes. Methuen, New York.
- Basaran, M, Uzun, O. and Erpul, G., 2017.** Evaluation of field performance of BEST aeolian sediment catcher in sandy-loam soil of arid zone of Turkey. *Soil and Water Res.*, Vol. 12, 96-105
- Cadée, G. 1992.** Eolian transport of Mya shells, *Palaios*, Vol. 7.
- Campos, L.D., 2018.** Quantification methods for aeolian sand transport on beaches. Doctoral Thesis, University of Twente, The Netherlands
- Davidson-Arnott, R.G.D., Yang, Y., Ollerhead, J., Hesp., P.A. and Walker, I.J., 2007.** The effects of surface moisture on aeolian sediment transport threshold and mass flux on a beach. *Earth Surface Processes and Landforms*, Vol. 33, 55-74. Doi:10.1002/esp.1527
- De Grande, E. and De Moor, T., 2019.** Influence of meteorological and environmental effects on aeolian transport (in Dutch). MSc. Thesis, KU Leuven, Belgium
- De Ruig, J.H.M., 1989.** De sediment balans van de Hollandse kust 1963-1986. Rapport GWAO-89.016 Dienst Getijdewateren, Rijkswaterstaat, Den Haag
- Dong, Z., Lu, P., Zhang, Z. and Qian, G., 2012.** Aeolian transport in the field: a comparison of the effects of different surface treatments. *Journal of Geophysical Research Atmosphere*, Doi: 10.1029/2012JD017538
- Farrell, E.J. and Swann, C.** *Geomorphological Techniques*. Chapter 3.1.4. British society for Geomorphology
- Ho, T., 2012.** Experimental study of saltating particles in a turbulent boundary layer. Doctoral Thesis, University of Rennes, France
- Han, Q., Qu, J., Liao, K., Zhu, S., Zhang, K., Zu, R. and Niu, Q., 2011.** A wind tunnel study of aeolian sand transport on a wetted surface using sands from tropical humid coastal southern China. *Environmental Earth Sciences*, Vol. 64, 1375-1385; DOI 10.1007/s12665-011-0962-7
- Kok, J.F., Parteli, E.J.R., Michaels, T.I. and Karam, D.B., 2012.** The physics of wind-blown sand and dust. *Rep. Prog. Phys.* Vol. 75, Doi:10.1088/0034-4885/75/10/106901
- Meyer-Peter, E. and Mueller, R., 1948.** Formulas for bed load transport. 2nd IAHR Congress, Stockholm, Sweden
- Nickling, W.G. and Davidson-Arnott, R.G.D., 1990.** Aeolian sediment transport on beaches and coastal dunes. *Proc. Canadian Symposium on coastal sand dunes*
- Poortinga, A, Van Minnen, J., Keijsers, J., Riksen, M., Goossens, D. and Seeger, M., 2013.** Measuring fast-temporal sediment fluxes with an analogue acoustic sensor: a wind tunnel study. *Plos One*, Volume 8, Issue 9, www.plosone.org
- Shao, Y. P. and Lu, H., 2000** A simple expression for wind erosion threshold friction velocity *Journal Geophysical Research* Vol. 105, 22437-43
- Sherman, D.J., Swann, C. and Barron, J.D., 2014.** A low-cost aeolian sand trap. *Aeolian Research*, Vol. 13, 31-34.
- Valance, A., Rasmussen, K.R., Moctar, A.O.E and Dupont, P., 2015.** The physics of aeolian sand transport. *Comptes Rendus Physique, Elsevier Masson*, Vol. 16 (1), 1-13. Doi: 10.1016/j.crhy.2015.01.006
- Van der Wal, D. 1998.** The impact of the grain-size distribution of nourishment sand on aeolian transport. *Journal of Coastal Research* Vol. 14 (2), 620-631
- Van Dijk, P. M. et al. 1996.** The influence of rainfall on transport of beach sand by wind. *Earth Surface Processes and Landforms*, Vol. 21, 341-352.
- Van Dijk, P.M. et al. 1999.** Aeolian processes across transverse dunes, part II. Modelling the sediment transport and profile development. *Earth Surf. Process. Landforms*. Vol. 24, 319-333